공학석사 학위논문

Performance Analyses for Conceptual Design of Hydrogen Fuel Cell Electric Aircraft

수소 연료전지 전기 항공기의 개념설계를 위한 성능해석

2023년 2월

서울대학교 대학원

항공우주공학과

이 종 윤

Performance Analyses for Conceptual Design of Hydrogen Fuel Cell Electric Aircraft

지도교수 이 복 직

이 논문을 공학석사 학위논문으로 제출함
2022년 12월

서울대학교 대학원
항공우주공학과
이 종 윤

이종윤의 공학석사 학위논문을 인준함
2022년 12월

위 원 장 이 관 중 (인)

부위원장 이 복 직 (인)

위 원 김 규 홍 (인)

Abstract

Performance Analyses for Conceptual Design of Hydrogen Fuel Cell Electric Aircraft

Jongyoon Lee
Aerospace Engineering
The Graduate School
Seoul National University

As climate change has emerged as a real threat to the existence of humankind, a worldwide movement of decarbonization, or the energy transition, is underway. The aviation industry, which accounts for about 3% of total carbon dioxide emissions as of 2019, is also required to transition to green mobility in line with this trend. Nowadays, fuel cell technology with green hydrogen is emerging as a promising carbon-free power source. A hydrogen fuel cell is expected to be used in aviation because it shows superior gravimetric energy, high energy efficiency, and low observability. However, some technical hurdles exist, such as low volumetric density and difficulty in storing. In this study, performance analyses of liquid hydrogen fuel cell aircraft for the conceptual design were performed to analyze its mission performance capabilities. The KC-100, a general aviation aircraft developed in South Korea, was adopted as a baseline airframe and modeled including the propeller. For the analysis of aerodynamic and propulsive performance, the vortex latex method, widely accepted aerodynamic methodology for the conceptual design stage, was adopted. The wind tunnel test results were analytically reproduced through the computational fluid dynamics to verify the aerodynamic model, and the results from the experiment and the computation were compared. Through this, the accuracy of the aerodynamic model was verified, and the analysis results were corrected. After

these, the aerodynamic and propulsion database was developed for the aircraft performance analysis. The weight estimation model of the fuel cell propulsion system was established to explore the change in weight of the electric aircraft compared to the baseline model, and the performance evaluation of the electric aircraft was conducted based on the newly derived weight. It was calculated that when about 45 kg of hydrogen was mounted based on the mission used in the study, the weight of the drug increased by about 11%.

Keywords: Electric aircraft, Fuel cell, Conceptual design, Liquid hydrogen, Electrification

Student Number: 2021-22099

Table of Contents

Abstract ..... **i**

Table of Contents ..... **iii**

List of Figures ..... **iv**

List of Tables ..... **vi**

Chapter 1. Introduction 1

1.1. Study Background 1

1.2. Cases of Fuel Cell Aircraft Development 4

1.3. Purpose of Research 7

Chapter 2. Method 8

2.1. Aircraft Modeling 8

2.2. Aerodynamic Analyses 10

2.3. Performance Analyses 13

2.4. Weight Estimation 19

Chapter 3. Results and Discussion 24

3.1. Panel Sensitivity Test 24

3.2. Aerodynamic Database Development 29

3.3. Propulsion Database Development 33

3.4. Weight Estimation 39

3.5. Performance Analyses 42

Chapter 4. Concluding Remarks 45

Bibliography 47

국문초록 51

List of Figures

Figure 1.1. Annual Increase of CO2 Emission from the Aviation Transport..... 2
Figure 1.2. Energy Density of Variable Energy Sources 2
Figure 1.3. Photo of the Boeing Fuel Cell Demonstrator..... 4
Figure 1.4. Photo of the ENFICA-FC 5
Figure 1.5. Photo of the Antares DLR-H2 5
Figure 1.6. Photo of the DLR HY4 6
Figure 2.1. Graphics of the KC-100 "Naraon" 8
Figure 2.2. KC-100 and Propeller Models on OpenVSP 10
Figure 2.3. The Amesim Simulation Model for the Mission Simulation 15
Figure 2.4. The Tafel Plots..... 17
Figure 2.5. Typical Polarization Curve Modeled in Simcenter Amesim 19
Figure 2.6. Schematic Diagram of Weight Estimation Approach..... 20
Figure 2.7. Flow Chart of Weight Estimation Model..... 23
Figure 3.1. Lifting Body Panel Distribution for Aspect Ratio 1:1 Model..... 24
Figure 3.2. Lifting Body Panel Distribution for Aspect Ratio 2:1 Model..... 24
Figure 3.3. Propeller Panel Distribution for Aspect Ratio 1:1 Model..... 25
Figure 3.4. Propeller Panel Distribution for Aspect Ratio 2:1 Model..... 25
Figure 3.5. Lift Coefficient Variance of Lifting Surfaces along the Number of Panels..... 26
Figure 3.6. Induced Drag Coefficient Variance of Lifting Surfaces along the Number of Panels 26
Figure 3.7. Elapsed Time versus Number of Panels for Lifting Surfaces..... 27
Figure 3.8. Thrust Coefficient Variance of Propeller along the Number of Panels 27
Figure 3.9. Power Coefficient Variance of Propeller along the Number of Panels 28
Figure 3.10. Elapsed Time versus Number of Panels for Propeller 28

Figure 3.11. Cessna 172 Model on OpenVSP 29
Figure 3.12. Lift Coefficient of Cessna 172 Calculated from VSPAERO and DATCOM 30
Figure 3.13. Drag Coefficient of Cessna 172 Calculated from VSPAERO and DATCOM 30
Figure 3.14. Pressure Coefficient Distribution along the Lifting Surface of KC-100 Model 31
Figure 3.15. Lift Coefficients of KC-100 Model 32
Figure 3.16. Drag Coefficients of KC-100 Model 32
Figure 3.17. Lift Coefficient Result of Unsteady Analysis 35
Figure 3.18. Drag Coefficient Result of Unsteady Analysis 35
Figure 3.19. VSPAERO Thrust Estimation Result 35
Figure 3.20. Lift Coefficient Result of Unsteady Analysis After Thrust Correction 36
Figure 3.21. Drag Coefficient Result of Unsteady Analysis After Thrust Correction 36
Figure 3.22. Propeller Performance Map with the Power Coefficient 38
Figure 3.23. Propeller Performance Map with the Thrust Coefficient 38
Figure 3.24. Mission Plot for the Weight Estimation 40
Figure 3.25. Fuel Consumption Rate and Mass Variance over Time 41
Figure 3.26. Flowchart of Performance Analysis 42
Figure 3.27. Performance Analysis Results of (a) Thrust, (b) Power, and (c) Rate of Climb 43

List of Tables

Table 1.1. Specifications of Previously Developed Fuel Cell Aircrafts..... 7
Table 2.1. Specification of KC-100 Aircraft..... 9
Table 2.2. Coefficients and Parameters for Weight Estimation Model..... 22
Table 3.1. Solver Validation Analysis Condition of Cessna 172 Case 29
Table 3.2. Experiment Setup of KC-100 Wind Tunnel Test..... 33
Table 3.3. VSPAERO Input Parameters for Propeller Model Validation..... 33
Table 3.4. Parameters of Mission Segment for the Weight Estimation 40
Table 3.5. Weight Estimation Result 41
Table 3.6. Cruise Speed Calculation Result..... 42
Table 3.7. Results of the Mission Performance Analysis..... 44

Chapter 1. Introduction

1.1. Study Background

These days, climate change caused by global warming is becoming an inescapable menace to the existence of humankind. As a result, the radical reform of the energy mix, which is often called an 'energy transition', has arisen as one of the urgent agendas for this century. The energy transition from a carbon-intensive structure to zero-carbon is compelled for most industry sectors[1].

As globalization progresses, the demand for aviation transportation is rapidly growing. As a result, the number of carried passengers increased from 2.25 billion seats (2009) to 4.56 billion seats (2019)[2].

Due to the increased air traffic, greenhouse gas emissions are also rising dramatically. As seen in Figure 1.1, CO2 emissions are increasing rapidly by more than 4% every year[4]. According to the ICCT (International Council on Clean Transportation), the aviation industry produced about 905 million tons of carbon dioxide, corresponding to around 2.9% of all human-included CO2 emissions. As a result, carbon dioxide emissions have increased by about 32% compared to five years ago[3,4].

Figure 1.2 shows various materials with their energy density and specific energy[5]. Lithium-ion battery, which is the most promising, shows about 250 Wh/L of energy density. It is significantly low compared to fossil fuel, which offers 9,500 Wh/L.

The steep rise in greenhouse gas emissions shows the need for decarbonization in the aviation sector. However, replacing fossil fuels with green energy is very challenging. It is essential to reduce structural weight and fuel weight for the perspective of securing the payload. Fossil fuels, such as aviation fuels, show high volumetric and gravimetric densities, which makes them irreplaceable.

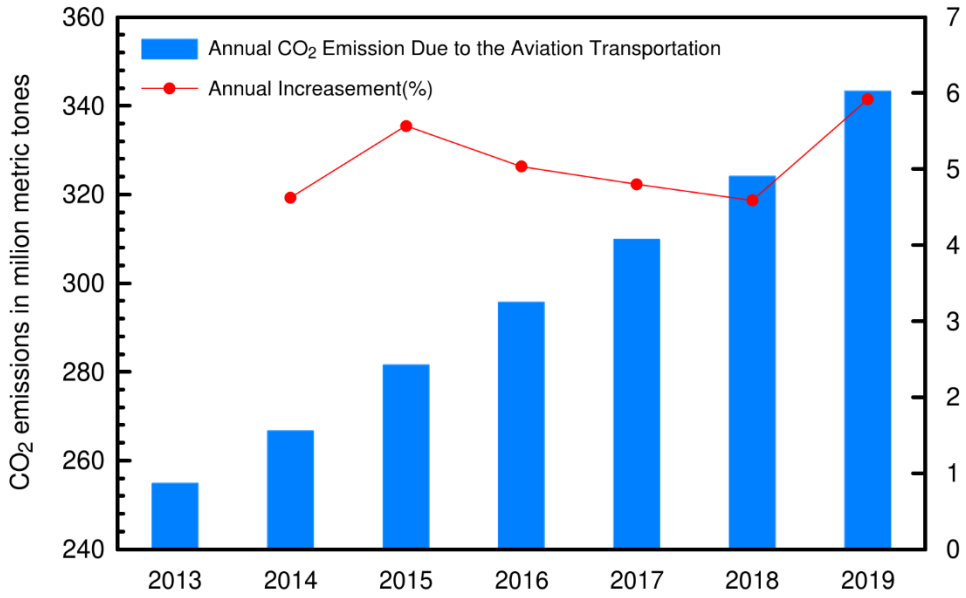

Figure 1.1. Annual Increase of CO2 Emission from the Aviation Transport

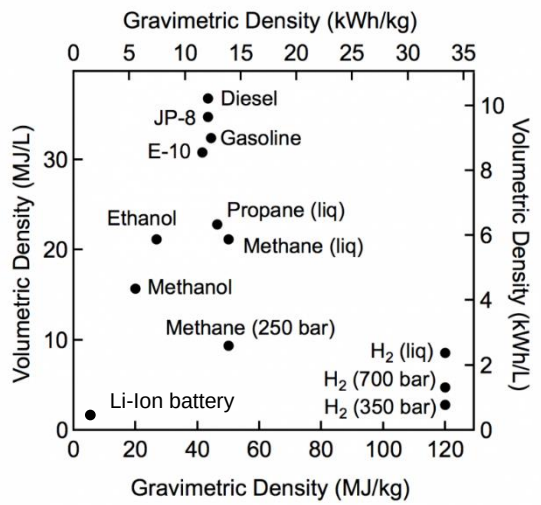

Figure 1.2. Energy Density of Variable Energy Sources

Consequently, to reduce the environmental effect of the aviation industry, the necessity of developing sustainable aviation fuels (SAFs), which might replace fossil fuels, has emerged. Various materials, including biofuel, e-Fuel, and hydrogen, are

widely studied today[1]. Among these candidates, hydrogen is one of the promising energy sources widely studied nowadays. With the advance of electrolysis technology, hydrogen can be produced carbon-neutrally, which is often called ‘green’ hydrogen. Also, utilizing hydrogen as a fuel produces no carbon dioxide at all. Hydrogen as a fuel can be utilized in two manners: direct combustion in the engine and feed for the fuel cell[6]. Considering technical readiness and compactness, a fuel cell has been extensively investigated as a substitute for an internal combustion engine in the transport sector.

After the adoption of the fuel cell for the space application during the Gemini earth-orbiting missions, fuel cells have received attention for aerospace applications because of their reliability, efficiency, and mission flexibility[7]. Today, proton exchange membrane fuel cells (PEMFCs) are thought to be the most promising candidates for the transport sector because of their superior energy density, low operating temperature, and fast response time[8]. Also, fuel cell aircraft are inherently carbon-neutral and have the advantage of low observability due to low noise and minimal heat generation of the fuel cell. These characteristics suggest that fuel cell aircraft can be used for military purposes.

However, some technical limitations take work to overcome to actualize hydrogen-powered aircraft. As aforementioned, the fuel cell powertrain and hydrogen storage system are still too bulky and heavy. Conventional aircraft keep their fuel inside the wing tank. However, liquid hydrogen cannot be stored in the same manner because of the multiple insulation layers. Also, compared to the fuel cell automobiles which are operated on earth, fuel cell at high altitude requires a large air compressor to keep the air supply. For this reason, fuel cell aircraft developed so far are UAVs (Unmanned Aerial Vehicles) or single-seater airplanes, which are very limited in size.

1.2. Cases of Fuel Cell Aircraft Development

The Boeing Fuel Cell Demonstrator was the first manned aircraft powered by a fuel cell[9,10]. The initial flight of the aircraft took place in 2008. The Diamond HK36 Super Dimona, a two-seater aircraft, was chosen as the baseline model, modified with a 75-kW fuel cell and with 1 kg of hydrogen compressed to 350 bar. In addition, a 75-kW output lithium-ion battery system was mounted to supply additional power for climb. In the early stages of development, aircraft were manufactured assuming liquid hydrogen to be used, but the plan was changed to use pressurized hydrogen because it was difficult to develop a lightweight cryogenic tank.

Figure 1.3 is a photo of the Boeing Fuel Cell Demonstrator[11].

Figure 1.3. Photo of the Boeing Fuel Cell Demonstrator

ENFICA-FC, an Environmentally Friendly Inter-City Aircraft powered by Fuel Cell, ran from 2007 to 2010[12]. The platform aircraft was Jihlavan Rapid 200 aircraft. ENFICA-FC had a maximum take-off weight of 554 kg and was equipped with about 1.2 kg of compressed hydrogen of 350 bar. It requires 40 kW of power during the climb stage, and the battery and fuel cell bear half of the power.

Figure 1.4 is a picture of the ENFICA-FC[12].

Figure 1.4. Photo of the ENFICA-FC

Unlike the two aforementioned aircraft, the Antares DLR-H2 is the first manned aircraft to receive energy only from fuel cells without battery assistance[13]. The project ran from 2008 to 2015, utilizing the Lange Aviation Antares 20E aircraft as its base model. DLR-H2 showed a maximum take-off weight of 750 kg and a power output of 40 kW. It is equipped with 4.9 kg of hydrogen compressed to 350 bar. The first-generation model developed in 2009 was equipped with HT-PEMFC (High-Temperature Polymer Exchange Membrane Fuel Cell) with an operating temperature of 100°C or higher, while the second-generation model developed in 2012 was equipped with LT-PEMFC (Low-Temperature Polymer Exchange Membrane Fuel Cell) with an operating temperature of 80°C.

Figure 1.5 is a photograph of the Antares DLR-H2.

Figure 1.5. Photo of the Antares DLR-H2

DLR HY4 was the first four-seat fuel cell aircraft[14]. Built by modifying Pipistriel Taurus G4 aircraft, HY4 was built in the form of a twin-fuselage for

hydrogen storage and 4 crews. The fuel cell and the battery provide 45 kW of power, respectively. The maximum take-off weight is about 1,500 kg. The first flight was done in 2016.

Figure 1.6 is a picture of the DLR HY4[14].

Figure 1.6. Photo of the DLR HY4

In addition to these general aviation class aircraft, research is being conducted to mount hydrogen fuel cells in various sizes of aircraft, from multicopters to regional jets. Some of those are Ion Tiger UAV developed by Naval Research Laboratory[15], Boeing Phantom Eye UAV[16], Alakai Skai VTOL[17], and Hyundai Motor Group Project N multicopter[18], which uses hydrogen fuel cells as power sources.

Table 1.1 summarizes the specifications of the Boeing Fuel Cell Demonstrator, ENFICA-FC, and Antares DLR H2[9-14].

Table 1.1. Specifications of Previously Developed Fuel Cell Aircrafts

	Boeing FC Demo.	**ENFICA-FC**	**Antares DLR H2**	**DLR HY4**
Project period	2002-2008	2006-2010	2008-2015	2015-
Platform aircraft	Diamond HK36 Super Dimona	Jihlavan Rapid 200	Large Aviation Antares 20E	Pipistriel Taurus G4
MTOW [kg]	860	554	750	1500
H_2 capacity	34 L (350 bar) 1 kg	52 L (350 bar) 1.2 kg	205 L (350 bar) 4.9 kg	300-400 bar
Cruise speed [km/h]	110	135	120	145
ROC [m/s]	1.3	2.5	2.5	N/A
Takeoff power [kW]	75	40	42	80

1.3. Purpose of Research

In this study, point-mass-based performance analyses were done with the fuel-cell-powered airplane. The baseline model was based on the traditional jet-fuel-powered general aviation airplane. Using the OpenVSP software, the geometry model of the baseline aircraft was obtained, including the propeller. Also, a low-fidelity, high-speed aerodynamic analysis technique that can be used in the conceptual design stage was developed. After constructing the aerodynamic and propulsion database, the weight variance of the aircraft was calculated including the amount of hydrogen required for the specific mission was calculated and the fuel cell propulsion system. Finally, the performance analysis of the fuel cell electric aircraft, considering the change in weight, was done.

Chapter 2. Method

2.1. Aircraft Modeling

In this study, the KC-100 “Naraon”, developed by Korea Aerospace Industries, LTD. (KAI), was chosen as the baseline model. The KC-100 is a four-seated, cantilever low wing, single engine propeller-driven airplane that is certified as KAS Part 23 class. Powered by a Continental IO-550-K engine, the KC-100 shows a continuous power rating of 250 kW. Its 3-blade constant-speed propeller has a diameter of 78 inches and a rotation speed of about 2,500 RPM. The maximum takeoff weight of the KC-100 is 3,600 lbs.

Figure 2.1. depicts KC-100 aircraft[19].

Figure 2.1. Graphics of the KC-100 "Naraon"

Specifications of the KC-100 are shown in Table 2.1[20].

Table 2.1. Specification of KC-100 Aircraft

Parameter	Value
Seats	4
Airworthiness Standards	KAS Part 23
Reference wing area	14.007 m^2
Reference chord length	1.267 m
Reference span length	11.455 m
Rating power	315 HP @ 2,500 RPM
Maximum Operating Altitude	25,000 ft
Maximum Takeoff Weight	1,633 kg

OpenVSP software was used to model the KC-100 aircraft. OpenVSP, which stands for Open Vehicle Sketch Pad, is an open-source aircraft design tool initially developed by NASA. Unlike general CAD software, which requires a user to input every dimension and constraint to model geometry properly, OpenVSP is specialized for parametric aircraft design by means of familiar design variables such as wing chord length, sweep angle, and sectional airfoil.

OpenVSP can involve the propeller effect by two means: (1) actuator disk model and (2) rotating blades model. To develop the propulsion database dealing with the propeller, the rotating blades model was accepted for this study. A high-quality geometric model of the propeller is essential to capture its aerodynamic behavior properly during unsteady simulation.

The wing was modeled by combining known information such as reference area, aspect ratio, span length, chord length, airfoil, sweep angle, taper ratio, and dihedral angle. For further detailed design, a three-sided drawing was also referred to.

Landing gear and support structures are ignored for the convenience of modeling.

While propeller modeling, reverse engineering was done to acquire chordwise distribution of sectional geometric parameters such as airfoil, twist angle, chord length, and skew. Figure 2.2 is the KC-100 and its propeller models on OpenVSP.

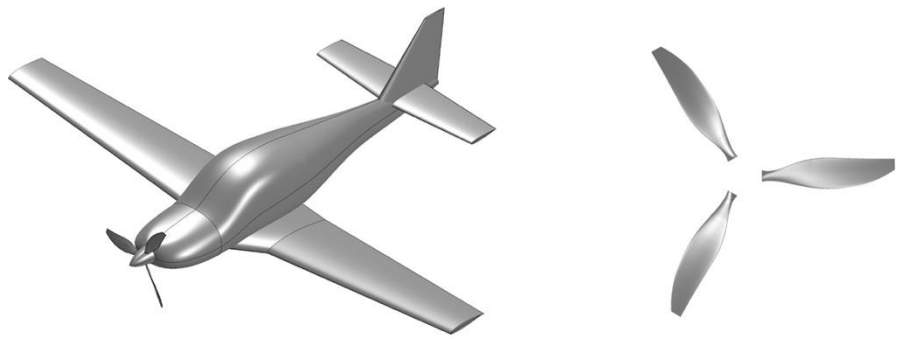

Figure 2.2. KC-100 and Propeller Models on OpenVSP

2.2. Aerodynamic Analyses

In this study, VSPAERO software was chosen as the aerodynamic solver for constructing aerodynamic databases. VSPAERO is a low-fidelity aerodynamic analysis tool provided with OpenVSP. It is a potential flow solver which provides two options for approaching the solution: (1) thick-surface panel method (PM) and (2) thin-surface vortex lattice method (VLM). Generally, the panel method is known to provide a more accurate solution compared to the VLM but shows much more computational cost[21].

VSPAERO requires the reference area of the main wing(Sref), reference span length (bref), reference chord length (cref), and coordinate of the center of gravity as geometric information, in addition to the geometry model.

VSPAERO also offers two models that can reflect the propeller effect, which is (1) the actuator disk model and (2) the rotating blade model. The actuator disk model is one of the fastest ways to evaluate propeller-driven aircraft performance, which ignores most of the geometric properties of the propeller. The power and thrust coefficient of the propeller are required inputs for the actuator disk model, which are generally assumed to be constant during the initial stage of design. To obtain power

and thrust coefficient, which are required to construct a propeller performance map, the rotating blade model is chosen. Knowing the detailed geometry of the propeller, including sectional airfoil, twist angle, and chord length, the rotating blade model is expected to show higher fidelity compared to the actuator disk model.

After modeling is done with OpenVSP, the aircraft geometry model is converted to an aerodynamic panel system (DegenGeom file) which is further utilized for VSPAERO aerodynamic solver. Panel distribution for the solver is controlled by *numU* and *numW* parameters defined for each part of the aircraft. Panel density can be adjusted by changing clustering near the leading edge and trailing edge for calculation efficiency.

For this study, VLM was selected because constructing a propulsion database involves a large number of unsteady flow solution cases with respect to advance ratio and propeller pitch angle.

VLM is a numerical approach for inviscid, irrotational flow. It is a widely accepted approach for finite-wing analysis in the early stage of aircraft design[22]. Based on the potential flow theory, VLM assumes the geometry as infinitely thin surface which is composed of small panels surrounded by vortex filaments. Those filaments induce aerodynamic force, and this phenomenon can be expressed by Biot-Savart's law.

The induced velocity of panel *i* by filament *j* is expressed as equation 2.1.

$$dw_{ij} = \frac{\Gamma_j}{4\pi}\frac{dl \sin\phi}{r^2} \tag{2.1}$$

Summing velocity induced by every filament can be expressed by introducing an influence coefficient matrix.

$$w_i = \sum_{j=1}^{N} A_{ij}\,\Gamma_j \tag{2.2}$$

Applying flow tangency condition, flow direction should be parallel with each panel. For small angle of attack, the equation can be written as equation 2.3.

$$w_i - v_i \tan\phi + V_\infty \left[\alpha - \left(\frac{dz}{dx}\right)_i\right] = 0 \tag{2.3}$$

Assuming planar wing, flow tangency condition can be rewritten in a simple form.

$$w_i + V_\infty \alpha = 0 \tag{2.4}$$

From equation 2.2 and 2.4, a solution for the strength of each vortex filaments can be found.

$$\sum_{j=1}^{N} A_{ij}\, \Gamma_j = -V_\infty \alpha \tag{2.5}$$

Applying Kutta-Joukoski theorem, lift generated from each panel can be found from the strength of the vortex filaments. Summing lift forces for each panel, lift generated from the wing can be determined.

$$L_i = \rho V_\infty \Gamma_i \tag{2.6}$$

$$L = \sum_{i=1}^{N} L_i \tag{2.7}$$

As seen in Figure 2.3, OpenVSP automatically convert 3D geometry file into planar computational domain which is required for VLM solver.

Detailed methodology of VLM can be found on the reference[23].

2.3. Performance Analyses

In the early stage of conceptual design, the point-mass assumption is usually adopted because of its simplicity.

Generally, a flight mission of a conventional takeoff and landing (CTOL) airplane is divided into 3 segments: climb, cruise, and descent.

Steady condition is assumed for the cruise segment. Assuming thrust is aligned with the flight path angle, thrust is compensated with drag, and lift is equal to gravity.

$$L = D \tag{2.8}$$

$$T = W \tag{2.9}$$

If the weight is known, lift force and lift coefficient can be found. As the lift coefficient can be considered as the linear function of the angle of attack, the angle of attack during the cruise segment can be drawn. As the angle of attack is known, the drag coefficient and force can also be determined.

The thrust required during the cruise can be calculated from the steady state assumption.

$$T_{\text{req}} = \frac{1}{2}\rho V_{\infty}^{2} C_D S_{\text{ref}} \tag{2.10}$$

Required power is a simple multiplication of required thrust and flight speed.

$$P_{\text{req}} = T_{\text{req}} V_{\infty} \tag{2.11}$$

During the climb and descent scenarios, where the altitude is linearly increasing or decreasing, excess power determines the rate of climb (ROC) or rate of descent (ROD). Excess power is the difference between available power and required power.

$$ROC = \frac{P_{\text{avail}} - P_{\text{req}}}{MTOW} \tag{2.12}$$

Available power is generally calculated by multiplying the engine power by the propulsion system efficiency.

There are three types of cruise speed: maximum endurance cruise, maximum range cruise, and economical cruise. At a maximum endurance condition, minimum power is required for aircraft to cruise steadily. At a maximum range condition, the required thrust becomes the least. In contrast, an economical cruise condition is achieved when the fuel consumption becomes the smallest, which means that the thrust-over-speed ratio is minimum. For this study, an economical cruise condition was adopted.

Aircraft weight is affected by loaded fuel mass and takeoff weight due to the fuel weight variance affecting the aircraft's performance. So, to find the exact fuel weight requirement, iterative simulation, or performance analysis, must be done.

Performance analyses are done with Simcenter Amesim software. Amesim is a scalable system simulation platform combined with ready-to-use multi-physics libraries such as mechanical, thermal, electrical, and fluid systems[24]. 1-D (point-mass), 2-D (longitudinal), and 3-D (6DoF) simulations of aircraft are available, and point-mass simulation was adopted for this study.

Figure 2.4 is the Amesim model developed for the study in order to perform mission simulation. Briefly, the Amesim simulation model consists of 8 submodels or subsystems: airplane body submodel, aerodynamic efforts submodel, propeller submodel, mission submodel, control subsystem, motor submodel, fuel cell submodel, and sensor subsystem.

The airplane body submodel defines a point body mass moving in space, according to Newton’s laws of motion. Thrust and aerodynamic forces are received to calculate the position, velocity, and flight angle of the aircraft.

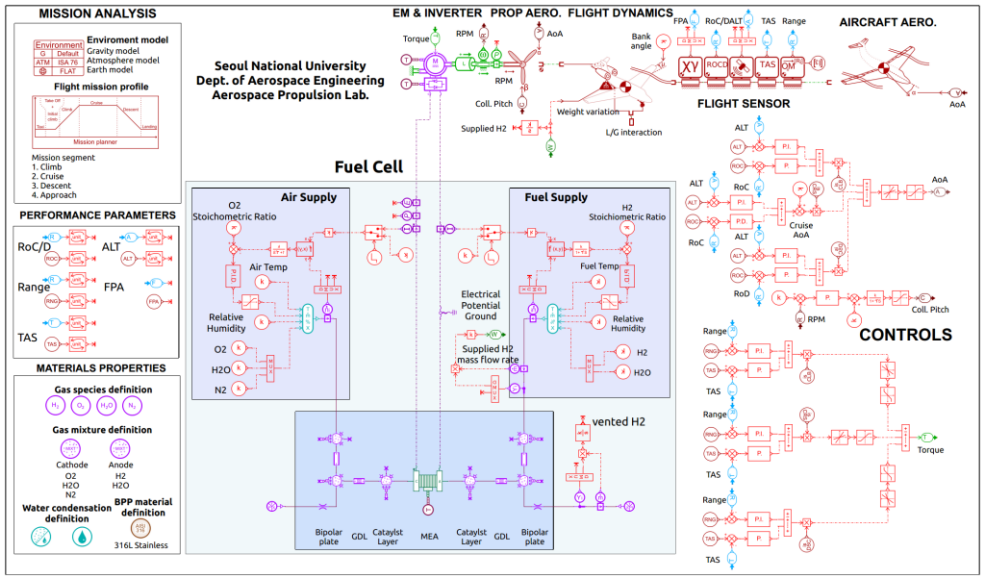

Figure 2.3. The Amesim Simulation Model for the Mission Simulation

The aerodynamic efforts submodel stores the aerodynamic database and provides aerodynamic forces to the body submodel. Propeller submodel stores propeller map data. The Propeller map consists of power and thrust coefficients according to the advance ratio and propeller pitch angle. The aerodynamic database and propeller map were established by the VSPAERO software aforementioned.

The mission submodel configures flight missions during each segment, such as climb, cruise, and descent. To make sure that the aircraft model follows the configured mission, the control subsystem, which is composed of multiple PID submodels, must be properly set.

The motor submodel converts torque and kinetic energy, which are required for the aircraft submodel to follow the configured mission, into current and voltage commands for the fuel cell submodel. The motor submodel is controlled with a torque signal generated from the control submodel.

To calculate power output of the fuel cell properly, the behavior of voltage and current from the cell must be modeled realistically. The current of the fuel cell is governed by the current density and the cell's active surface area. The voltage of the

fuel cell is rather complicated to describe. Generally, the cell voltage is calculated by subtracting the irreversibilities from the ideal reversible voltage.

$$V_{\text{cell}} = E_{\text{cell}} - (\eta_{\text{act}} + \eta_{\text{ohmic}} + \eta_{\text{concen}}) \tag{2.13}$$

Ideal reversible voltage is often referred to as open circuit voltage. Open circuit voltage (OCV), or reversible voltage, is the maximum available voltage while Gibbs free energy released by the fuel cell is fully converted to the electrical work. When partial pressures of the reactants are variant over time, effects of the activities (similar to the reaction constants) must be included to describe OCV. Nernst equation shows the relation between ideal cell voltage (or Nernst potential) and ion concentrations.

$$E_{\text{cell}} = E_{\text{Nernst}} = E^{o}_{\text{Nernst},c}(P_0, T) + \frac{RT}{nF}\log\frac{a_c}{a_a} \tag{2.14}$$

where n is the number of electrons released by the single hydrogen atom during the reaction, which is equal to 2. R is the gas constant, and F is the Faraday constant (about 96,500 C/mol). E^{o} is the Nernst standard potential at a reference pressure, which equals 1.23 V under 25℃ atmospheric conditions. a_c and a_a are the chemical activities at the cathode and anode, respectively.

The concept of 'overpotential' is involved to describe the irreversibilities of cell voltage and consists of activation loss, ohmic loss, and concentration loss[25].

Activation loss is induced by the finite reacting speed over the electrode surfaces. The overpotential is proportional to the logarithm of current density during the electrochemical reaction, and its relationship is called as Tafel equation.

$$\eta = A\ln\left(\frac{i}{i_0}\right) \tag{2.15}$$

As shown in Figure 2.5[25], overpotential is linear to the logarithm of current and the slope represents the reaction rate.

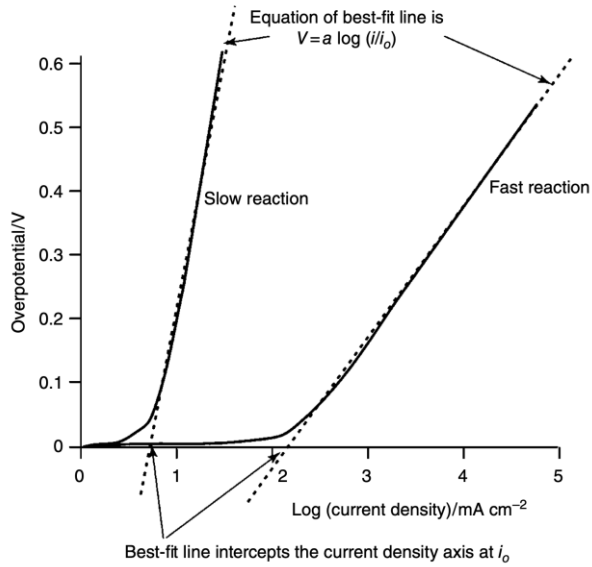

Figure 2.4. The Tafel Plots

To describe nonlinearity near low-current region, Butler-Volmer equation, expressed as equation 2.16, is widely adopted to describe the activation loss.

$$\eta_{\text{act}} = \frac{RT}{\alpha_c F}\ln\left(\frac{i}{i_{o,c}}\right) - \frac{RT}{\alpha_a F}\ln\left(\frac{i}{i_{o,a}}\right) \tag{2.16}$$

$$\frac{i_c}{i_{o,c}} = \exp\left(\frac{\eta_{\text{act},c}}{R}\left(\frac{1}{T_0}-\frac{1}{T}\right)\right)\left(\exp\left(\frac{\alpha_c nF\eta_{\text{act},c}}{RT}\right) - \exp\left(\frac{(1-\alpha_c)nF\eta_{\text{act},c}}{RT}\right)\right)\left(\frac{C_{O_2,c}}{C^*_{O_2,c}}\right)^{\gamma_{O_2}}\left(\frac{C_{H_2O,c}}{C^*_{H_2O,c}}\right)^{\gamma_{H_2O}} \tag{2.17}$$

$$\frac{i_a}{i_{o,a}} = \exp\left(\frac{\eta_{\text{act},a}}{R}\left(\frac{1}{T_0}-\frac{1}{T}\right)\right)\left(\exp\left(\frac{\alpha_a nF\eta_{\text{act},a}}{RT}\right) - \exp\left(\frac{(1-\alpha_a)nF\eta_{\text{act},a}}{RT}\right)\right)\left(\frac{C_{H_2,a}}{C^*_{H_2,a}}\right)^{\gamma_{H_2}} \tag{2.18}$$

where C is the concentration, α is the charge transfer coefficient, η_{act} is the activation energy of reaction for each electrode, and γ is the partial order.

Ohmic loss comes from the resistances of the electrodes. A linearly decreasing tendency of cell voltage is induced by the ohmic loss.

$$\eta_{\text{ohmic}} = R_{\text{memb}} \cdot j'_{\text{memb}} \tag{2.19}$$

Lastly, concentration loss, often referred to as mass-transport loss, is due to the insufficient supply of reactants to the electrode surface. Empirically, overpotential due to concentration loss is proportional to the exponential of the cell current. Thus, concentration loss causes a nonlinear drop in cell voltage in the high-current region. In Simcenter Amesim, concentration loss is thought to be taken into account in the activation voltage drop terms.

$$\eta_{\text{concen}} = m \exp(ni) \tag{2.20}$$

Combining equations 13-20, a polarization curve can be drawn and Amesim calculates the required cell voltage and current according to the curve for power output demanded the fuel cell submodel.

As fuel cell load is determined, consumed hydrogen during the flight can be determined by following Faraday's laws of electrolysis.

$$dn_{\text{H2}} = -\frac{I_{\text{stack}}}{nF} N_{\text{cell}} SR_{\text{H2}} \tag{2.21}$$

$$W_{\text{H2,consumed}} = \int MW_{\text{H2}}\ dn_{\text{H2}} \tag{2.22}$$

where SR_{H2} is the stochiometric ratio of hydrogen, n is the number of electrons emitted during the reaction, N_{cell} is the number of cells for stack, and MW_{H2} is the molecular weight of the hydrogen.

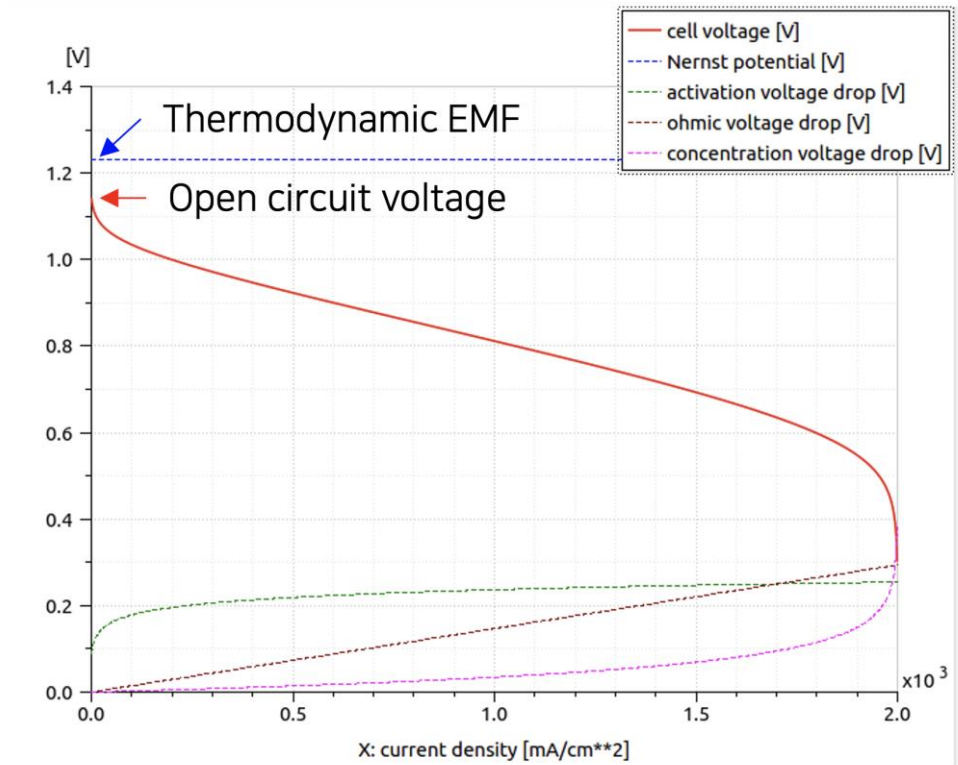

Figure 2.5. Typical Polarization Curve Modeled in Simcenter Amesim

2.4. Weight Estimation

During the conceptual design of an aircraft, weight estimation is generally performed in a textbook-based bottom-up manner. In the case of a fossil-fuel-based airplane, there is plenty of available information about the relationship or trend of required power and weight. Based on this information, the weight for each part of the airplane can be initially guessed, such as wings, fuselage, and power train.

However, estimating the weight of electricity-powered aircraft based on traditional methodology is inadequate because of the few precedence cases.

In this study, it is assumed that the piston engine drive system was detached in the base model aircraft and replaced by the fuel cell propulsion system.

Figure 2.6 is a schematic diagram of the weight estimation approach.

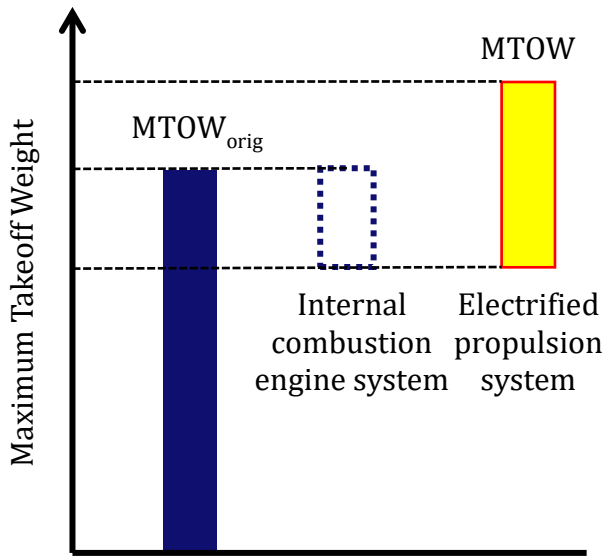

Figure 2.6. Schematic Diagram of Weight Estimation Approach

Engine, gearbox, and aircraft oil in the maximum mounted state were assumed to be piston engine driving systems. The weight of these parts was obtained from KC-100 specification report[19].

Weight estimation of the fuel cell propulsion system was done by bottom-up methodology. The propulsion system includes a fuel cell stack and its balance of the plant (BOP), a motor, hydrogen fuel, and hydrogen storage.

Equation for the aircraft mass calculation is represented as equations 2.23 and 2.24.

$$MTOW = MTOW_{\text{orig}} - W_{\text{ICEsys}} + W_{\text{H2,loaded}} + W_{\text{tank}} + W_{\text{FCsys}} \tag{2.23}$$

$$MTOW = MTOW_{\text{orig}} - (W_{\text{fuel}} + W_{ICE}) + \left(W_{\text{H2,consumed}} \cdot \frac{1}{1-\mu_{\text{heel}}} \cdot \left(1 + \frac{1}{\mu_{\text{tank}}}\right) + W_{\text{FCsys}}\right) \tag{2.24}$$

where μ_{heel} is tank heel ratio, which is the ratio of unusable because of the physical limitation of the tank. μ_{tank} is the storage efficiency of liquid hydrogen. For this study,

tank heel was assumed to be 5%[27] and liquid hydrogen storage efficiency was to be 7.5 wt%[28].

A fuel cell system consists of a fuel cell stack and BOP, which can be made up of a hydrogen supply system, air supply system, and thermal management system.

Since there is little information available on the weight of the liquid hydrogen fuel cell system, the weight estimation method developed in the previous study was applied. Park et al.[26] performed market research and derived a trend equation that calculates the weight of each element of the fuel cell system from the output power required for the fuel cell and the amount of hydrogen required.

Fuel stack weight was assumed to be linearly increasing with the required power. Fuel cell stacks developed by Horizon Fuel Cell Technology were chosen as the model data.

$$W_{\text{stack}} = \alpha P_{FS} + \beta \tag{2.25}$$

An air supply system (ASS) was modeled with the specific weight of the humidifier and the air compressor.

$$W_{ASS} = P_{FS}\left(SP_{\text{humid}} + SP_{\text{aircomp}}\right) \tag{2.26}$$

Linearity was assumed for the weight of a hydrogen supply system (HSS) with the required storage for hydrogen fuel.

$$W_{HSS} = \kappa_1 W_{\text{tank}} \tag{2.27}$$

Lastly, the size of a thermal management system (TMS) was supposed to increase with released heat, which is affected by the maximum output of the fuel stack.

$$W_{TMS}(kg) = 0.5526 \times P_{\text{rejected}}(kW) - 3.9818 \tag{2.28}$$

$$P_{\text{rejected}}(kW) = \kappa_2 P_{FS} \tag{2.29}$$

Coefficients and parameters used for the study are presented in Table 2.2[26].

Table 2.2. Coefficients and Parameters for Weight Estimation Model

Parameter	Value
α	0.3938 kg/kW
β	19.737 kg
SP_{humid}	0.03375 kg/kW
$SP_{aircomp}$	0.275 kg/kW
κ_1	0.137623
κ_2	1.105

Sizing of hydrogen fuel cells mounted on Hyundai Motor's NEXO vehicle was performed to verify the fuel cell system weight estimation model. In the case of the 95 kW NEXO hydrogen fuel cell, the stack weight was calculated to be about 155.9 kg when using the model. This is a result predicted to be about 20% lower than the actual weight of 187 kg[29].

As the amount of hydrogen loaded increases, the takeoff weight of the aircraft increases, which affects the aircraft's performance, such as fuel consumption rate and rate of climb. In contrast, with insufficient hydrogen fuel, the range of aircraft can be affected. So, optimization of the required hydrogen fuel is necessary. The optimal aircraft weight was derived by repeated analysis through Amesim simulation. With iterative simulation, a minimal amount of fuel was found. Figure 2.7 is a schematic diagram of the iterative analysis.

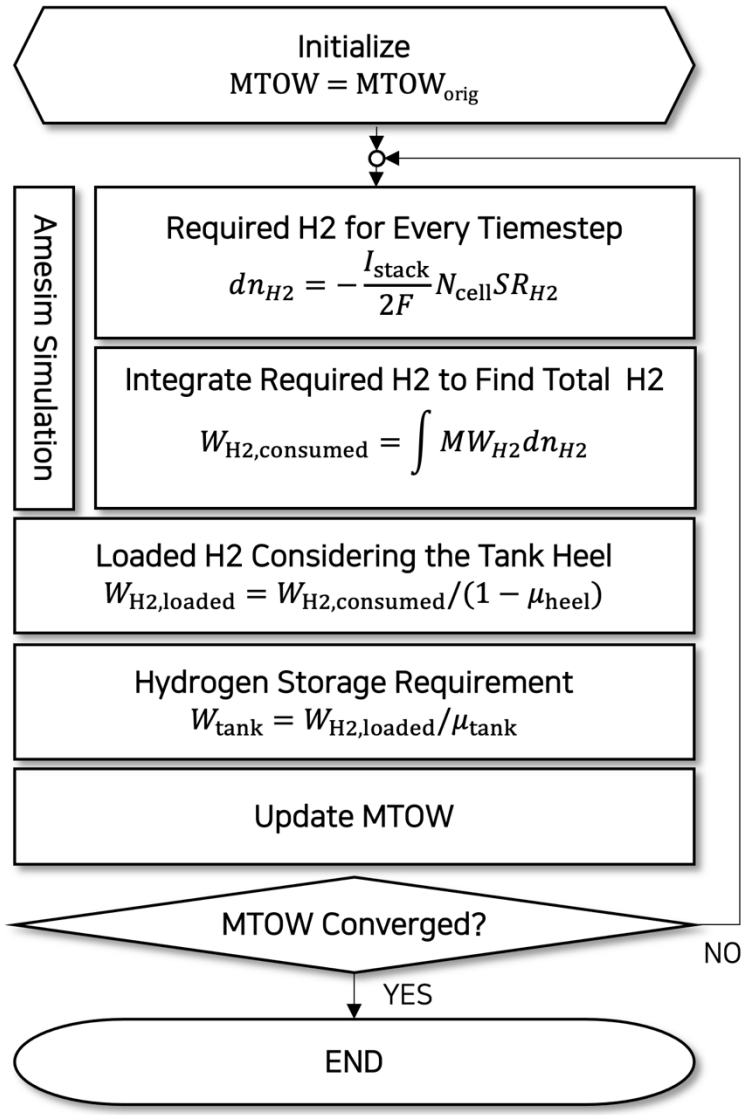

Figure 2.7. Flow Chart of Weight Estimation Model

Chapter 3. Results and Discussion

3.1. Panel Sensitivity Test

In order to prevent the configuration of the panel system from affecting the aerodynamic analysis result, a panel sensitivity test was performed. Based on the idea suggested by Sheridan et al.[30], not only the number of panels but also the aspect ratio of the panel was considered.

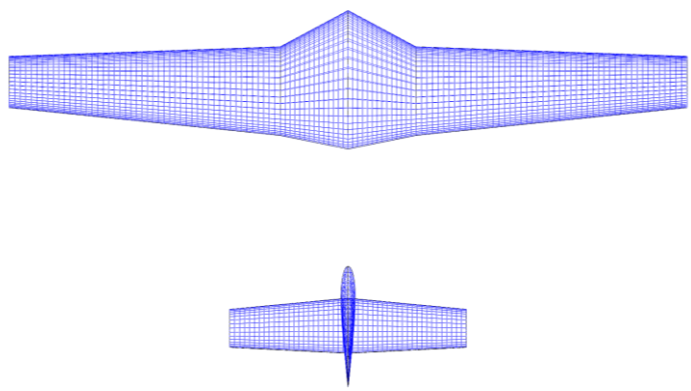

Figure 3.1. Lifting Body Panel Distribution for Aspect Ratio 1:1 Model

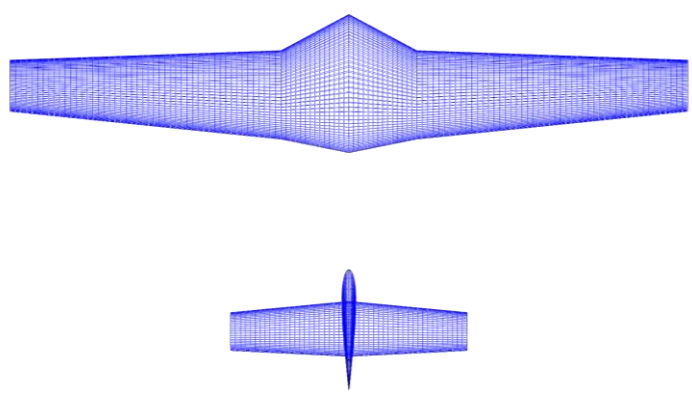

Figure 3.2. Lifting Body Panel Distribution for Aspect Ratio 2:1 Model

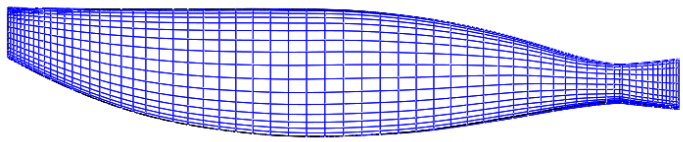

Figure 3.3. Propeller Panel Distribution for Aspect Ratio 1:1 Model

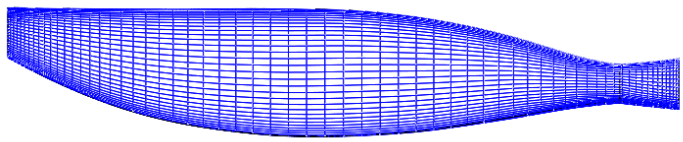

Figure 3.4. Propeller Panel Distribution for Aspect Ratio 2:1 Model

For both wing and propeller, two types of panel systems with an aspect ratio of about 1:1 and 2:1 near the center of the geometry were modeled. By varying the number of panels, the lift coefficient and drag coefficient of the wing and the power coefficient and the thrust coefficient of the propeller were calculated, respectively. Also, for leading edges and tail edges, denser panel distribution is applied to capture the aerodynamic effect properly. The optimal panel system was selected in consideration of the convergence of each coefficient and the time required for calculation.

Figures 3.1 and 3.2 represent the panel distribution for the aspect ratio 1:1 and 2:1 model, respectively. Similarly, Figures 3.3 and 3.4 are propeller panel distributions.

As a result of the analysis, it was found that the model with an aspect ratio of 2:1 shows faster calculation speed compared to the aspect ratio 1:1 model. Therefore, the aspect ratio 2:1 model was adopted as the baseline model. Models with 42,340 panels and 3,200 panels were chosen as baseline panel systems for the wing and propeller, respectively. Results of the panel sensitivity test can be found in Figures from 3.5 to 3.10.

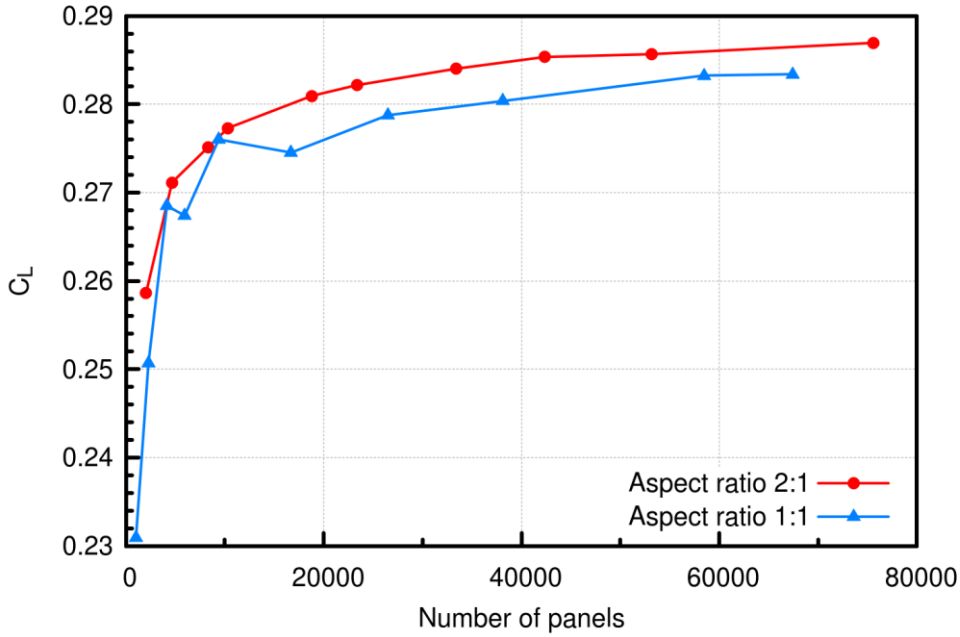

Figure 3.5. Lift Coefficient Variance of Lifting Surfaces along the Number of Panels

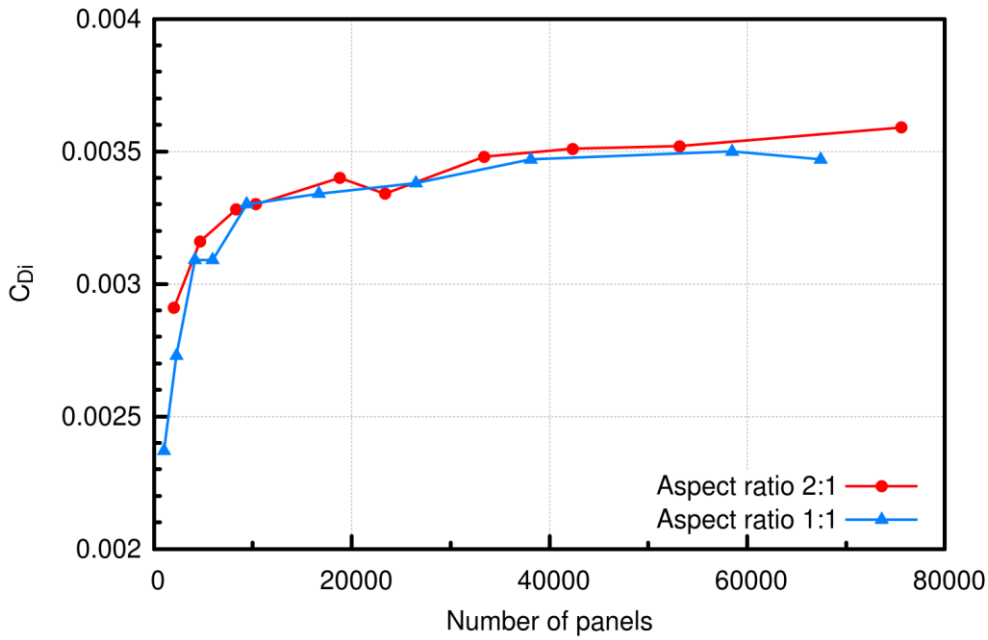

Figure 3.6. Induced Drag Coefficient Variance of Lifting Surfaces along the Number of Panels

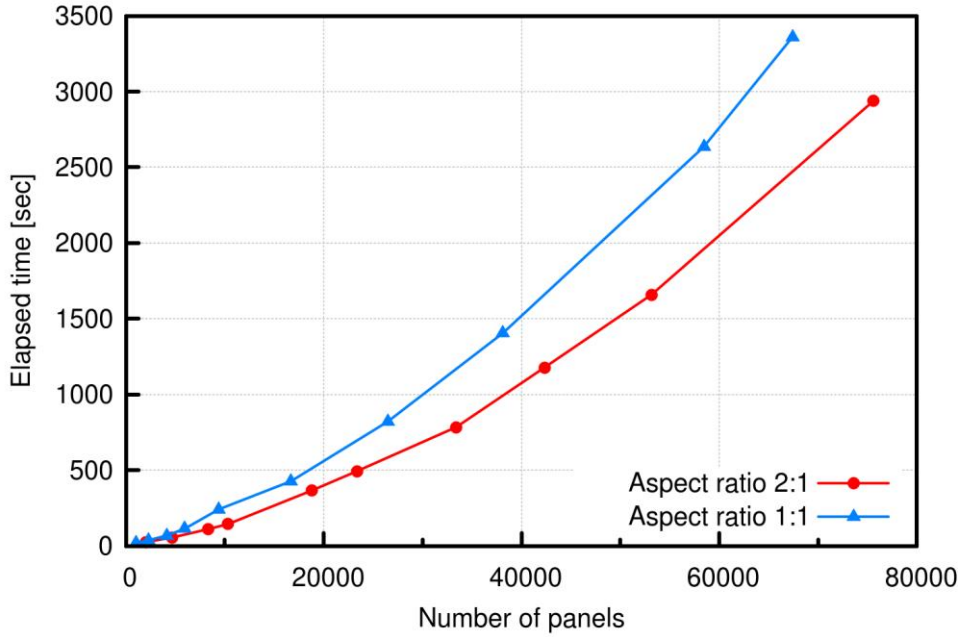

Figure 3.7. Elapsed Time versus Number of Panels for Lifting Surfaces

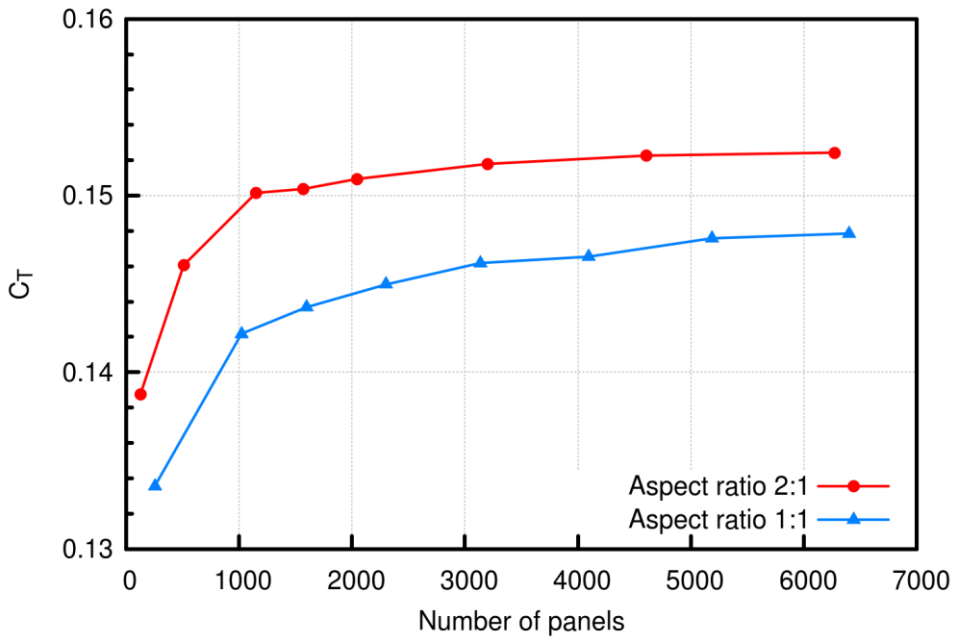

Figure 3.8. Thrust Coefficient Variance of Propeller along the Number of Panels

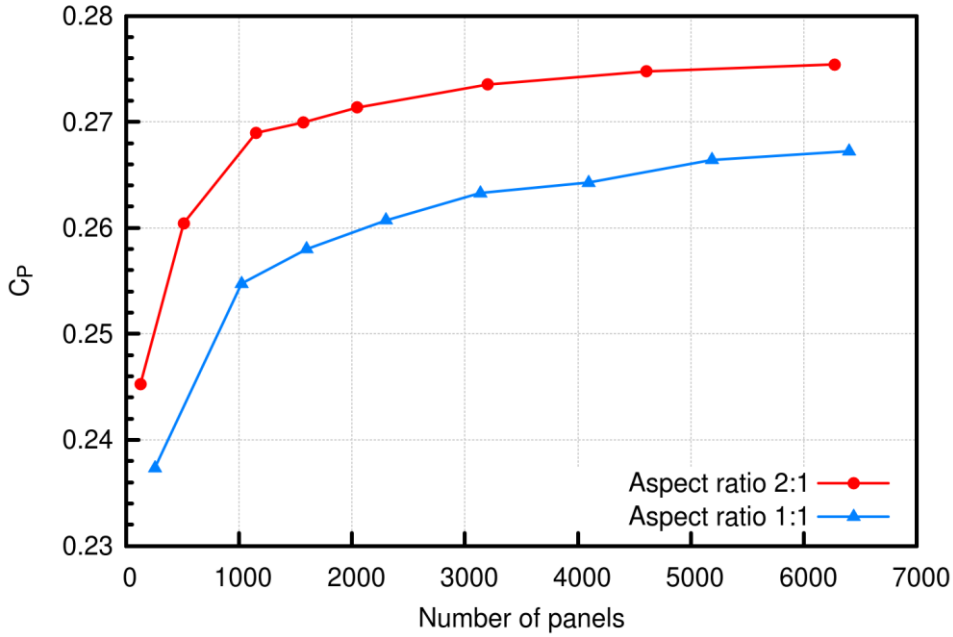

Figure 3.9. Power Coefficient Variance of Propeller along the Number of Panels

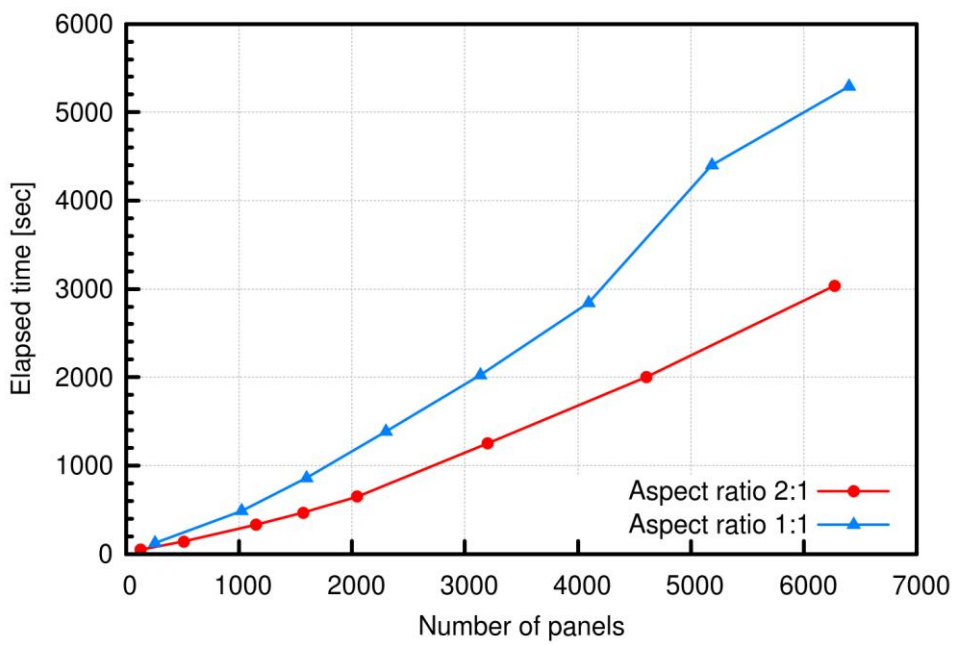

Figure 3.10. Elapsed Time versus Number of Panels for Propeller

3.2. Aerodynamic Database Development

To import the aerodynamic performance of aircraft, the lift coefficient and drag coefficient were calculated with varying angles of attack.

For constructing an aerodynamic database, only the lifting surfaces and fuselage were considered without the propeller.

To verify the accuracy of VSPAERO, the famous Cessna 172 aircraft was chosen as a validation case. The geometry file is acquired via the VSP Hangar, the web repository maintained by the OpenVSP provider, and shown in Figure 3.11.

For comparison, DATCOM aerodynamic analysis result was acquired.

The aerodynamic analysis condition is summarized in Table 3.1.

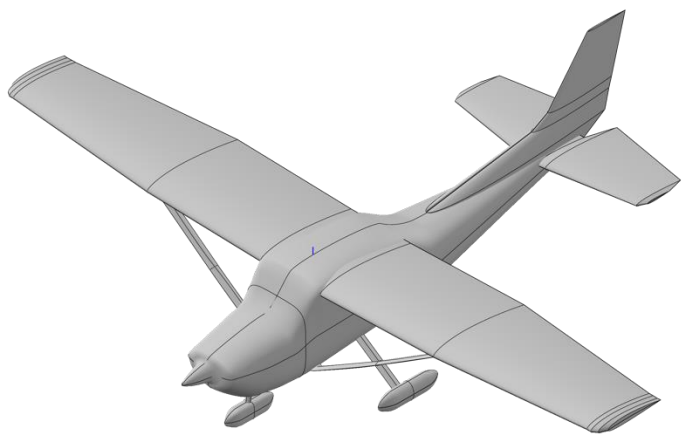

Figure 3.11. Cessna 172 Model on OpenVSP

Table 3.1. Solver Validation Analysis Condition of Cessna 172 Case

Parameter	Value
Angle of attack, α	-10° ~ 20°, (1° interval)
Freestream velocity, V_{inf}	100 m/s
Mach number, Ma	0.16
Reynolds number, Re_{Cref}	3,235,900

Figures 3.12 and 3.13 are lift and drag coefficient calculated from VSPAERO and DATCOM, respectively. The aerodynamic coefficients calculated from VSPAERO and DATCOM were similar before the pre-stall region, except for the zero-lift drag or parasite drag.

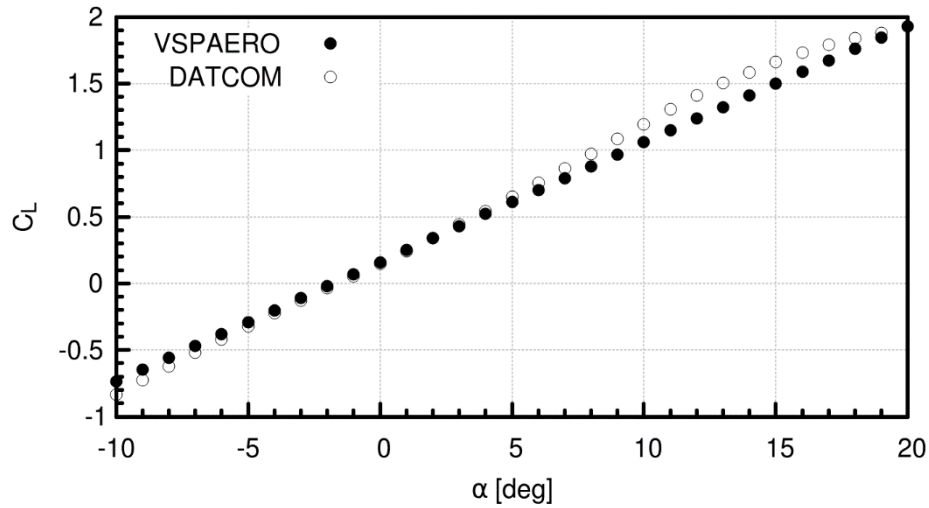

Figure 3.12. Lift Coefficient of Cessna 172 Calculated from VSPAERO and DATCOM

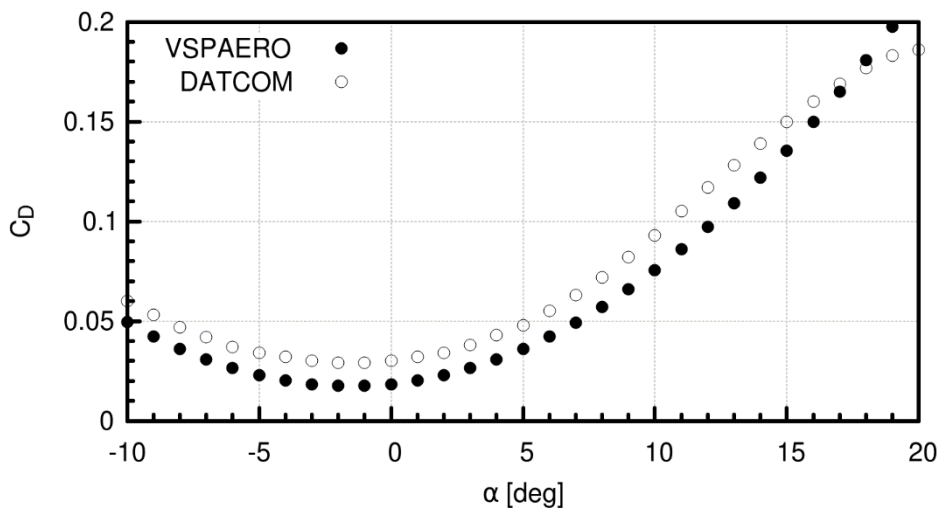

Figure 3.13. Drag Coefficient of Cessna 172 Calculated from VSPAERO and DATCOM

After verification of the VSPAERO solver, the aerodynamic database of the KC-100 model was constructed. Aerodynamic coefficients were compared with the wind tunnel data obtained from the KC-100 development report[19].

Since the parasite drag estimation of VSPAERO is based on the simple textbook-based build-up method, parasite drag should be corrected or re-calculated. The build-up method can induce considerable error in the general aviation airplane, so the estimation of excrescence drag should be reflected. Based on the research done by Pfeiffer and Lednicer[31], parasite drag calculated from VSPAERO was assumed to be estimated 15% higher than the true value, and the correction was done.

Figure 3.14 shows the coefficient of pressure distribution along the KC-100 model. Figures 3.15 and 3.16 show the aerodynamic database developed for this study.

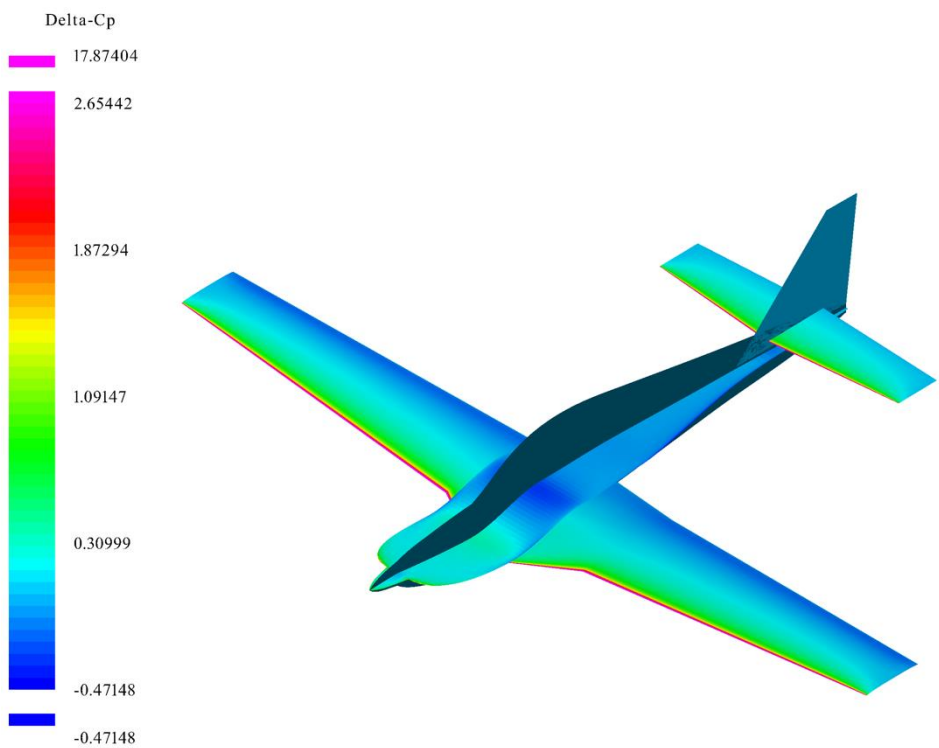

Figure 3.14. Pressure Coefficient Distribution along the Lifting Surface of KC-100 Model

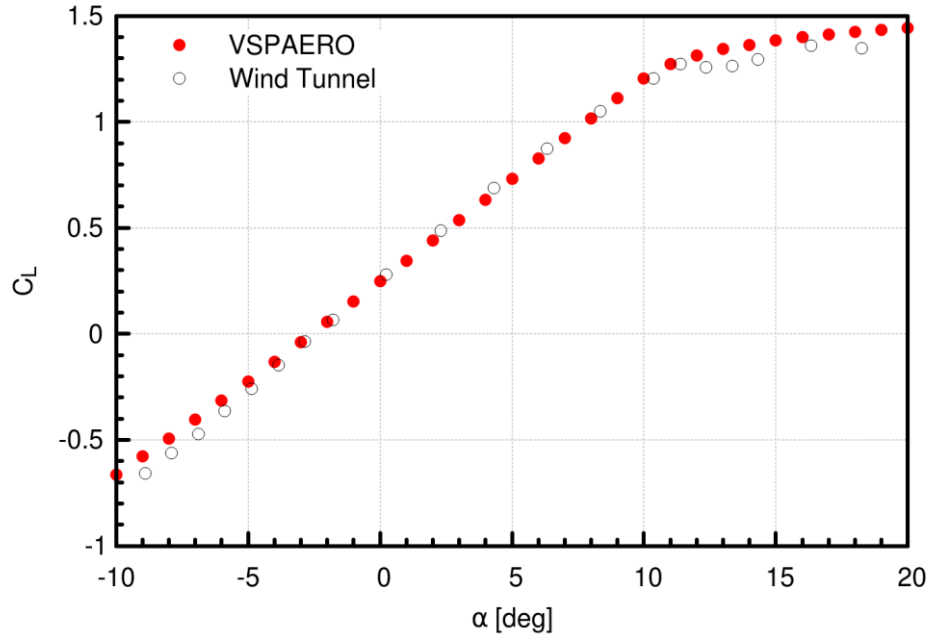

Figure 3.15. Lift Coefficients of KC-100 Model

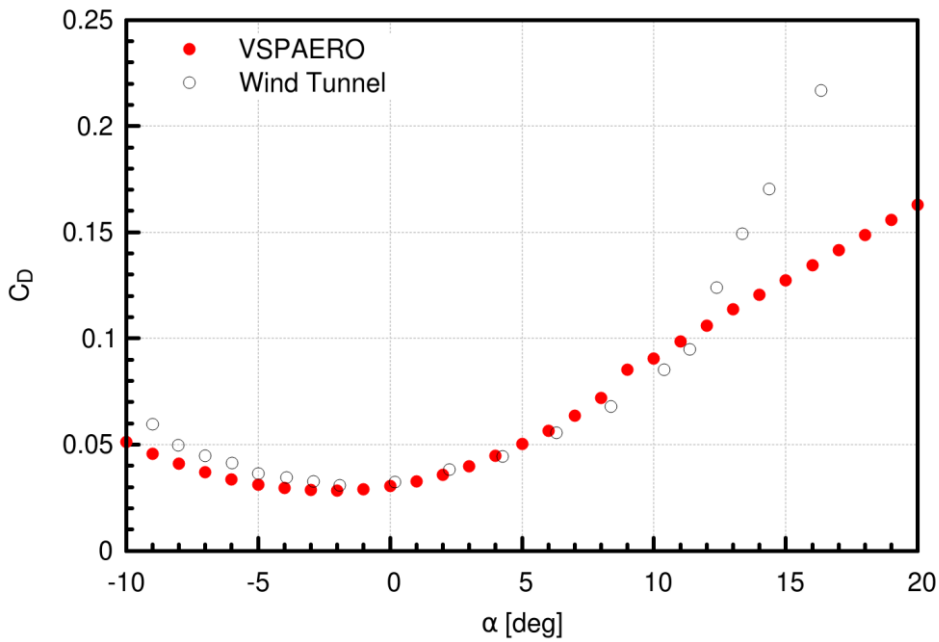

Figure 3.16. Drag Coefficients of KC-100 Model

3.3. Propulsion Database Development

To build the propulsion database of the propeller of the KC-100 model, verification of the thrust calculation model of VSPAERO was conducted. The wind tunnel test data measuring the aerodynamic force with a rotating propeller was compared with the result of the unsteady analysis of the integrated airframe-propeller model calculated from VSPAERO.

The flow condition of the wind tunnel test is shown in Table 3.2[19]. Since the reduced model of 20% scale was used for the wind tunnel test, the flow condition for the actual scale model were induced from the dimensionless number. Input parameters of VSPAERO unsteady analyses for propeller model validation are presented in Table 3.3.

Table 3.2. Experiment Setup of KC-100 Wind Tunnel Test

Parameter	Case 1	Case 2	Case 3
Advance ratio	0.5048	0.6525	0.8226
Blade angle	23.1°	24.8°	27.0°
V_{CAS}	81.0 knots	104.7 knots	132 knots
V_{test}	25 m/s	25 m/s	25 m/s
Motor rotational speed	7500 RPM	5800 RPM	4600 RPM

Table 3.3. VSPAERO Input Parameters for Propeller Model Validation

Parameter	Case 1	Case 2	Case 3
Angle of attack, α	-10° ~ 20°	-10° ~ 20°	-10° ~ 20°
Advance ratio	0.5048	0.6525	0.8226
Freestream velocity, V_{inf}	41.67 m/s	53.86 m/s	67.91 m/s
Reynolds number, Re_{Cref}	2.1532×10^{6}	4.6793×10^{6}	5.8994×10^{6}
Motor rotational speed	2500 RPM	2500 RPM	2500 RPM

In the case of VSPAERO, the aerodynamic forces acting on each body part, such as the airframe and propeller, can be analyzed separately. However, in the case of the wind tunnel test, it is almost impossible to separate the aerodynamic forces generated by the propeller, the fuselage, and the lift. To compare aerodynamic forces reasonably, an equation was derived to calculate the net force acting on the entire aircraft and applied to the VSPAERO result data.

A propeller rotating in one direction inevitably induces a moment. To offset the moment, the propeller is mounted with a downward and rightward angle, which is called a down-thrust angle and a right-thrust angle, respectively. For KC-100, since an angle of 2° was applied for both the down-thrust and right-thrust angle, the corresponding mounting angle was reflected in the electric force conversion equation.

The conversion equations for lift and drag are as follows.

$$C_L = C_{L,\text{plane}} + \frac{T\cos(i_r)\sin(\alpha - i_d)}{\frac{1}{2}\rho V_\infty^2 S_{\text{ref}}} \tag{3.1}$$

$$C_D = C_{D,\text{plane}} - \frac{T\cos(i_r)\cos(\alpha - i_d)}{\frac{1}{2}\rho V_\infty^2 S_{\text{ref}}} \tag{3.2}$$

Figures 3.17 and 3.18 depict the aerodynamic coefficients calculated with VSPAERO and the coefficients obtained from the wind tunnel test.

In the case of drag coefficients, about 60% of differences were observed, which are affected by the VSPAERO's tendency of thrust overestimation. For further investigation, the propulsion performance of the isolated propeller was combined with the aerodynamic performance of the lifting body obtained from the wind tunnel result, which is described in Chapter 3.2, to review the accuracy of the propeller analysis model. As seen in Figure 3.19, overestimation of drag coefficients is mainly due to the miscalculation of thrust by VSPAERO instead of the lifting body effect.

Based on this result, calibration of reducing thrust was done by dividing 1.6 for propeller thrust and power, respectively.

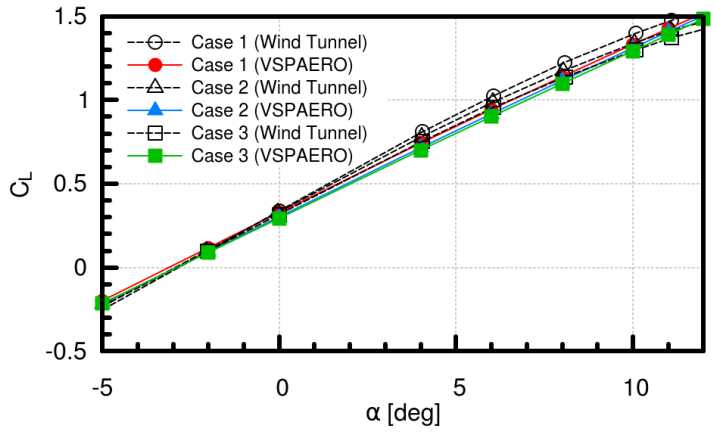

Figure 3.17. Lift Coefficient Result of Unsteady Analysis

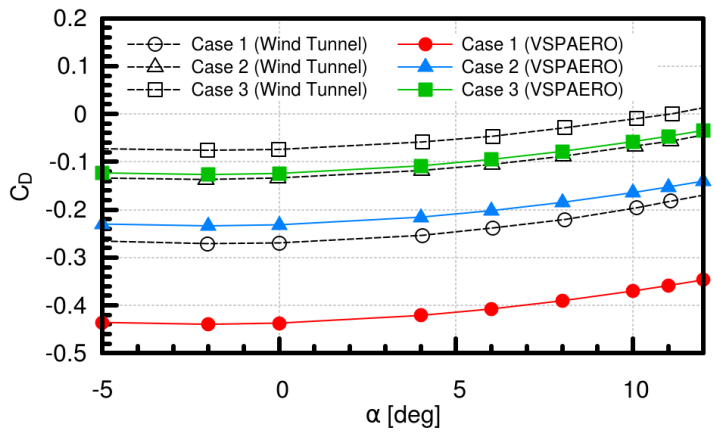

Figure 3.18. Drag Coefficient Result of Unsteady Analysis

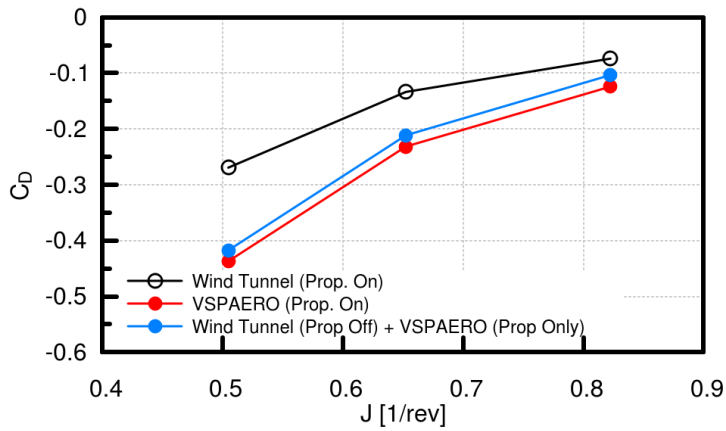

Figure 3.19. VSPAERO Thrust Estimation Result

Corrected lift drag coefficients are presented in Figure 3.20 and 3.21.

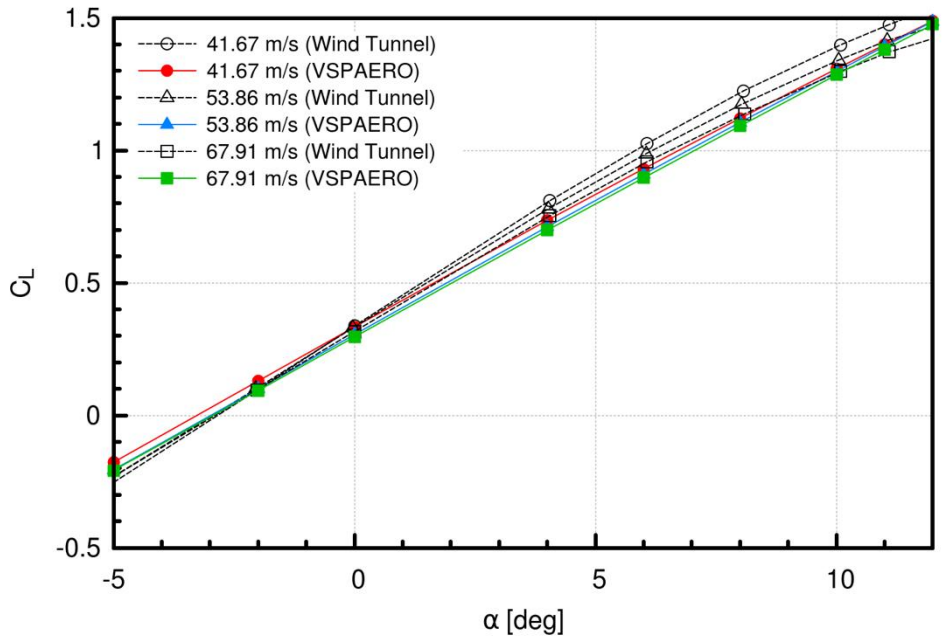

Figure 3.20. Lift Coefficient Result of Unsteady Analysis After Thrust Correction

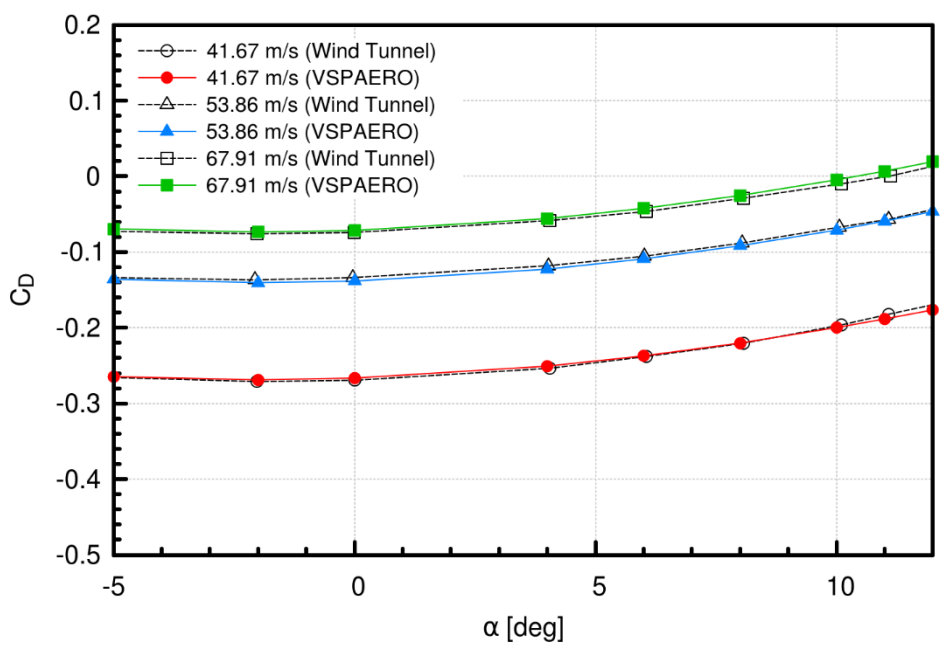

Figure 3.21. Drag Coefficient Result of Unsteady Analysis After Thrust Correction

After verifying the capability of VSPAERO for calculating aerodynamic forces, the KC-100 propulsion database, or the propeller performance map, was developed. The analysis conditions for database construction are shown in Table 3.4.

Table 3.4. Flow Condition and Propeller Configuration for Propeller Performance Map Development

Parameter	Value
Angle of Attack, α	0°
Propeller pitch angle, $\beta_{3/4}$	15° ~ 35° (5° interval)
Freestream velocity, V_{inf}	50 m/s ~ 200 m/s (10 m/s interval)
Atmospheric density, ρ	1.225 kg/m^3

The propeller performance map usually consists of the thrust coefficient, power coefficient, and propulsive efficiency, varying with the propeller pitch angle and the advance ratio. Parameters for propeller performance can be defined as below:

$$C_T \equiv \frac{T}{\rho n^2 D^4} \tag{3.3}$$

$$C_P \equiv \frac{P}{\rho n^3 D^5} \tag{3.4}$$

$$\eta_P \equiv \frac{TV}{2\pi nQ} = J\frac{C_T}{C_P} \tag{3.5}$$

Figure 3.22 represents the propulsion efficiency according to the forward ratio, pitch angle, and power efficiency. Figure 3.23 shows the propulsion efficiency according to the forward ratio, pitch angle, and thrust efficiency. Simcenter Amesim requires propulsion efficiency as a function of power coefficient as Figure 3.22.

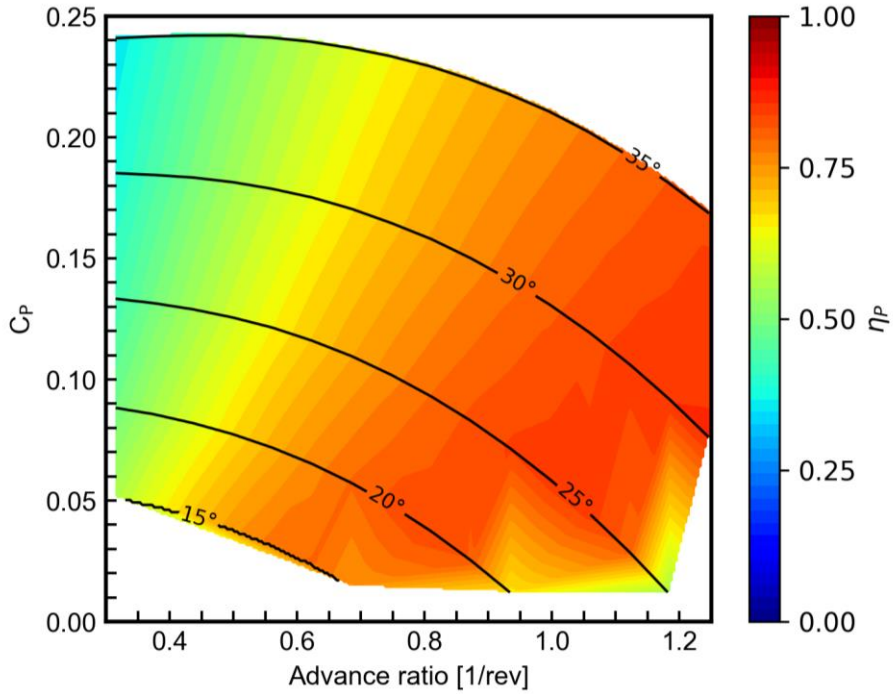

Figure 3.22. Propeller Performance Map with the Power Coefficient

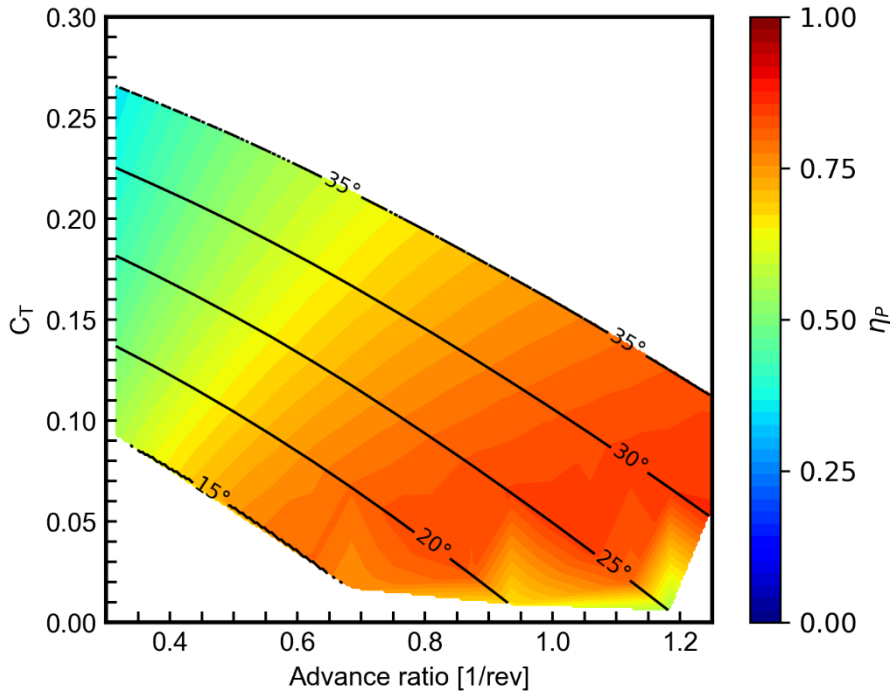

Figure 3.23. Propeller Performance Map with the Thrust Coefficient

3.4. Weight Estimation

Aircraft weight estimation was performed using the hydrogen fuel cell propulsion system weight estimation model presented by Park et al.[26] aforementioned. To perform mission-based weight estimation, iterative simulations were done using Simcenter Amesim software to calculate the weight of the hydrogen fuel required.

To construct the mission, the baseline aircraft's performance was analyzed. The available power was assumed to be 70% of the maximum power of the fuel cell, and the cruise altitude was set to 12,000 ft.

Assuming 100% throttle when climbing, the operating point exists during the climb where the effect on altitude is minimal. The rate of increase was calculated using the cruising speed and required power at this time. As a result, the rate of climb of 1,410 fpm (7.16 m/s) at a flight speed of 106 KTAS (196 km/h) was assumed as the climb segment.

The economic cruise condition is achieved at the point where the ratio of required thrust relative divided by cruise speed is minimal, as mentioned earlier. At a cruising altitude of 12,000 ft, the point at which this value is the minimum was determined as the cruise speed, which corresponds to approximately 152 knots (282 km/h).

In the descent and approach section, the freestream velocity was assumed to be 106 KTAS, the same as the climb segment. It was assumed that 20% of the available power was assumed during the descent, showing a performance of 310 fpm (1.57 m/s) at the descent rate and that it had an approach angle of 3° when approaching from 2,000 ft to the ground.

An initial mission diagram for the weight estimation of aircraft is composed as shown in Figure 3.24. Table 3.4 shows the operating conditions of the aircraft at each mission segment.

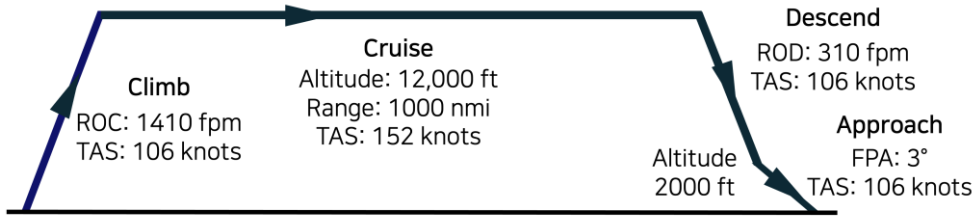

Figure 3.24. Mission Plot for the Weight Estimation

Table 3.4. Parameters of Mission Segment for the Weight Estimation

Mission Segment	Parameter	Value	Unit
Climb (15 min)	Rate of climb	800	ft/min
	Equivalent airspeed	90	knot
Cruise (66.7 min)	Altitude	12,000	ft
	Range	155.73	nmi
	True airspeed	140	knot
Descend (33.3 min)	Rate of descent	300	ft/min
	Equivalent airspeed	116.57	knot
	Target altitude	2000	ft
Approach (4.2 min)	Flight path angle	3	degree
	True airspeed	90	knot

Iterative calculations were performed to calculate the hydrogen fuel load of the aircraft to perform the above mission, and the results are summarized in Table 3.5. Takeoff weight was calculated to be 1812.68 kg. The weight variation of the fuel-cell-powered aircraft was +179.7 kg, which is 11% increase compared to the baseline model. The loaded hydrogen weight was calculated to be about 43.3 kg. It corresponds to 17.3% of the KC-100 oil tank capacity, which is 250 kg.

Table 3.5. Weight Estimation Result

Iteration No.		$M_{H2,consumed}$ [kg]	$M_{H2,loaded}$ [kg]	M_{FCtank} [kg]	M_{FCsys} [kg]	Initial Weight [kg]	Final Weight [kg]
0	-	-	-	-	1633		1589.56
1	43.44	45.726	259.12	379.80	1830.64		1789.22
2	41.421	43.601	247.07	378.14	1814.81		1773.63
3	41.184	43.351	245.66	377.95	1812.96		1771.81
4	41.146	43.311	245.43	377.92	1812.66		1771.51
5	41.148	43.314	245.45	377.92	1812.68		1771.53

Figure 3.25 shows the hydrogen fuel consumption rate and aircraft weight variance over elapsed time.

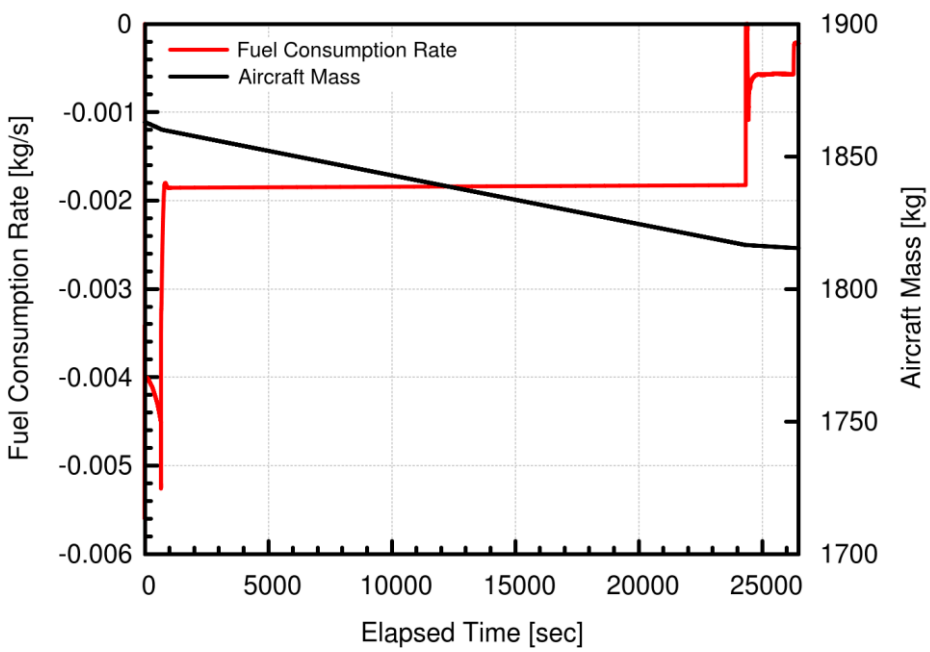

Figure 3.25. Fuel Consumption Rate and Mass Variance over Time

3.5. Performance Analyses

The performance analyses of the aircraft were performed based on the takeoff weight calculated from the aircraft weight estimation.

The analysis was performed by applying the methodology presented in Chapter 2.3. Figure 3.26 summarizes the performance analysis process.

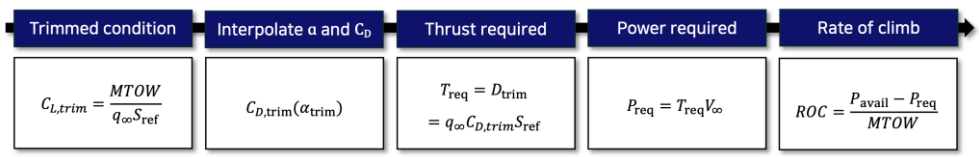

Figure 3.26. Flowchart of Performance Analysis

It is assumed that the aircraft climbs from sea level to an altitude of 12,000 ft (FL120). The thrust and power requirement and rate of climb varying with the cruise speed were analyzed at the two altitude conditions, and are shown in Figure 3.27, respectively.

As mentioned earlier, there are three main categories of cruising speeds: maximum endurance, maximum range, and economic cruise. Table 3.6 summarizes the results of the cruise speed calculation. In this study, economical cruise condition was adopted.

Table 3.6. Cruise Speed Calculation Result

Operating point	Condition	V_{cruise}
Maximum endurance cruise	Minimum power required	94.5 knots
Maximum range cruise	Minimum thrust required	116.5 knots
Economical cruise	Minimum fuel consumed (Minimum T/V_∞)	153 knots

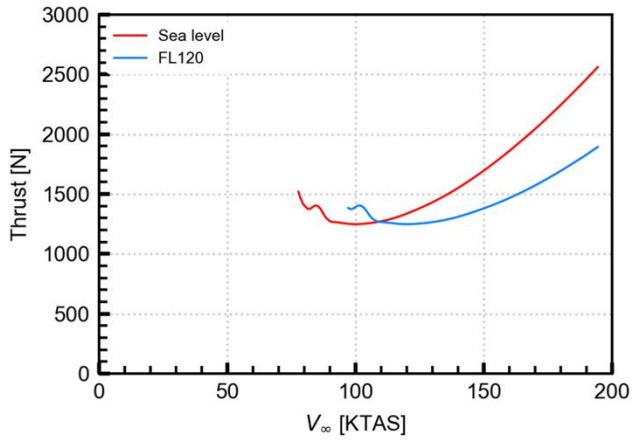

(a)

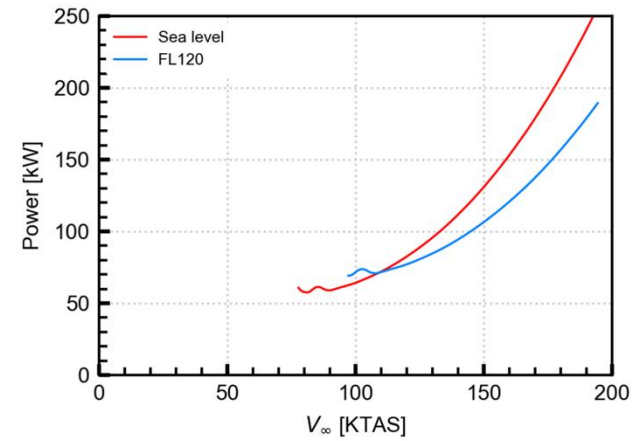

(b)

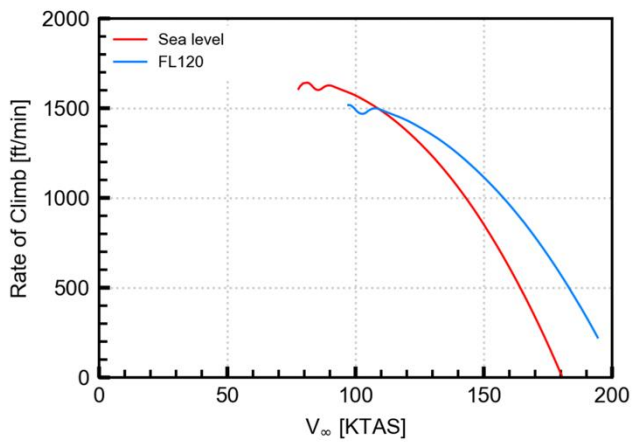

(c)

Figure 3.27. Performance Analysis Results of (a) Thrust, (b) Power, and (c) Rate of Climb

The rate of climb of an aircraft is derived from the difference between the available power and the required power. ROC was analyzed by assuming the available power as 70% of the maximum fuel cell power.

The optimal ROC was assumed to be the point where the influence of the altitude change is minimized.

Table 3.7 summarizes the results of the mission performance analysis.

Table 3.7. Results of the Mission Performance Analysis

Mission parameter	Value
Minimum power required	63.1 kW
Cruise speed (economical cruise)	153 knots
Maximum rate of climb	1282 ft/min
Airspeed at maximum rate of climb	94.5 knots

Chapter 4. Concluding Remarks

As the global trend of decarbonization demands a change in the aviation industry, Hydrogen fuel cell is emerging as a promising future fuel. This research aimed to explore the feasibility of fuel-cell-powered aircraft and introduced hydrogen fuel cells and evaluate the mission performance of the fuel cell aircraft. The KC-100 aircraft developed in Korea was adopted as a baseline airframe, and the fuel cell propulsion system was retrofitted. The aerodynamic and propulsion database of aircraft was constructed using the vortex lattice method. The variation of weight due to the electrification of the propulsion system was calculated, and the mission performance was evaluated based on the renewed takeoff weight.

One of the limitations of this study is the verification of the hydrogen fuel cell weight estimation model. The weight estimation at the conceptual design stage is usually obtained by statistically estimating the weight of each part and system from a previously developed aircraft and summing it up in a bottom-up manner. However, it is currently almost impossible to find published weight information for hydrogen fuel cell propulsion systems. This is partly because the current fuel cell is often mounted on the ground vehicle, so weight is not the biggest problem for design. It is expected that the accuracy of the weight model will also be improved as the available data for hydrogen fuel cells increases in the future.

In addition, in the case of hydrogen, the energy density is low. So, when loading a large amount, not only the weight but also the volume must be considered. In the case of liquid hydrogen storage, a high insulation performance requirement and a hydrogen supply system must be required, resulting in considerable weight and mounting space. Therefore, hydrogen fuel should be optimized by considering the constraints caused by the mounting space during the actual aircraft's design, and the optimal cruise range and mission plot should be constructed from these design constraints.

Currently, numerous companies around the world are interested in hydrogen propulsion systems. In Korean Peninsula, there is practically zero fossil fuel buried, so an absolute majority of its energy sources depend on imports. Taking energy transformation as an opportunity, pursuing energy security by investing in clean energy-based industries, including the aviation field, is suggested.

Bibliography

[1] Lee, J., and Lee, B. J., "Survey on Research and Development of E-Fuel," Journal of The Korean Society Combustion, Vol. 27, No. 1, 2022, pp. 37-57.

[2] World Bank. “Air transport, passengers carried.” The World Group Bank. Accessed December 13, 2022. https://data.worldbank.org/indicator/IS.AIR.PSGR.

[3] Global Carbon Project. "Annual carbon dioxide (CO_2) emissions worldwide from 1940 to 2021 (in billion metric tons)." Chart. November 11, 2022. Statista. Accessed January 31, 2023. https://www.statista.com/statistics/276629/global-co2-emissions/

[4] IATA. "Carbon Dioxide Emissions From Commercial Aviation Worldwide From 2004 To 2022 (In Million Metric Tons)." Chart. October 5, 2021. Statista. Accessed January 31, 2023. https://www.statista.com/statistics/1186820/co2-emissions-commercial-aviation-worldwide/

[5] US Department of Energy. “Hydrogen Storage.” Hydrogen and Fuel Cell Technologies Office. Accessed May 20, 2022. https://www.energy.gov/eere/fuelcells/hydrogen-storage

[6] Wentz, W., Myose, R., and Mohamed, A., “Hydrogen-Fueled General Aviation Airplanes,” AIAA Paper 2005-7324, September 2005.

[7] Warshay, M., and Prokopius, P. R., “The Fuel Cell in Space: Yesterday, Today and Tomorrow,” NASA TM-102366, September 1989.

[8] Sharaf, O.Z., and Orhan, M.F., “An Overview of Fuel Cell Technology: Fundamentals and Applications,” *Renewable and Sustainable Energy Reviews*, Vol. 32, 2014, pp. 810-853.

[9] Lapeña-Rey, N., Mosquera, J., Bataller, E., and Ortí, F., "The Boeing Fuel Cell Demonstrator Airplane," SAE Technical Paper 2007-01-3906, 2007.

[10] Lapeña-Rey, N., Mosquera, J., Bataller, E., and Ortí, F., ″First Fuel-Cell Manned Aircraft,″ *Journal of Aircraft*, Vol. 47, No. 6, 2010, pp. 1825-1835.

[11] Boeing, “A Green Machine,” Boeing Frontiers, 2008. p. 4.

[12] Romeo, G., Borello, F., Correa, G., and Cestino, E., “ENFICA-FC: Design of Transport Aircraft Powered by Fuel Cell & Flight Test of Zero Emission 2-Seater Aircraft Powered by Fuel Cells Fueled by Hydrogen,” *International Journal of Hydrogen Energy*, Vol. 38, 2013, pp. 469-479.

[13] German Aerospace Center, “Antares DLR-H2: Take-Off with the Power of Fuel Cells,” TT-EC-0412-S-F-018.

[14] German Aerospace Center. "HY4- Zero-emission Passenger Flights.” Accessed January 31, 2023. https://www.dlr.de/tt/en/desktopdefault.aspx/tabid-10743/

[15] Swider-Lyons, K., Schuette, M., Stroman, R., Rodgers, J., Page, G., and Mackrell, J., “Liquid Hydrogen Fuel System for Small Unmanned Air Vehicles,” AIAA 2011-6975, September 2011.

[16] Mills, G. L., Buchholtz, B., and Olsen, A., “Design, Fabrication and Testing of a Liquid Hydrogen Fuel Tank for a Long Duration Aircraft,” *Advances in Cryogenic Engineering*, Vol. 1434, No. 1, 2012, pp. 773-780.

[17] Electric VTOL News, “Alaka’i Technologies Skai,” Accessed January 31, 2023. https://evtol.news/alakai-technologies-skai/

[18] Pulse, “Hyundai Motor unveils Project N, first regional air mobility flying longer than UAM,” May 26, 2022. Accessed January 31, 2023.

[19] 한국항공우주산업, “소형항공기급 인증기 개발 최종보고서,” December 2013.

[20] 대한민국 국토교통부, “KC-100 형식증명자료집,” ACTC201301, March 2013.

[21] Shahid, T., Sajjad, F., Ahsan, M., Farhan, S., Salamat, S., and Abbas, M., “Comparison of Flow-Solvers: Linear Vortex Lattice Method and Higher-Order Panel Method with Analytical and Wind Tunnel Data,” 3rd International Conference on Computing, Mathematics and Engineering Technologies, Sukkur, Pakista, January 2020.

[22] White, F. M., “Fluid Mechanics,” 8th ed., McGraw-Hill Education, 2016.

[23] Bertin, J. J., and Cummings, R. M., “Aerodynamics for Engineers,” 6th ed., Pearson, 2014.

[24] Siemens PLM, “Simcenter Amesim: Optimize System Performance from Early Design Stages,” Accessed December 22, 2022. https://www.plm.automation.siemens.com/global/en/products/simcenter/simcenter-amesim.html

[25] Dicks, A., and Rand, D., “Fuel Cell Systems Explained,” 3rd ed., Wiley, 2018.

[26] Park, J., Lee, D., Lim, D., and Yee, K., “A Refined Sizing Method of Fuel Cell-Battery Hybrid System for eVTOL Aircraft,” *Applied Energy*, Vol. 328, 2022, p. 120160.

[27] Ahluwalia, R. K., Papadias, D. D., Peng, J-K, and Roh, H. S., “System Level Analysis of Hydrogen Storage Options,” U.S. DOE Hydrogen and Fuel Cells

Program 2020 Annual Merit Review and Peer Evaluation Meeting, Washington, DC, May 2020.

[28] Rivard, E., Trudeau, M., and Zaghib, K., "Hydrogen Storage for Mobility: A Review," *Materials*, Vol. 12, 2019, p. 1973.

[29] Hyundai Motors, "Hyundai Fuel Cell System," January 2021. Accessed January 31, 2023. https://hyfindr.com/wp-content/uploads/2022/01/Atch1-Hyundai-Fuel-Cell_ebrochure.pdf

[30] Sheridan, C. N., Pham, D. D., and Whiteside, S., "Evaluation of VSPAERO Analysis Capabilities for Conceptual Design of Aircraft with Propeller-Blown Wings," AIAA 2021-2510, July 2021.

[31] Pfeiffer, N. J., and Lednicer, D., "A Study of Airplane Excrescence Drag," AIAA 2014-2866, June 2014.

국 문 초 록

기후변화가 인류의 존속에 실질적인 위협으로 다가오면서, 전세계적인 탈탄소화 운동이 진행되고 있다. 2019 년 기준 전체 이산화탄소 배출량의 약 3%를 차지하는 항공 산업 역시 이러한 기조에 발맞추어 그린 모빌리티로의 이행을 요구받고 있다. 현재 대표적인 무탄소 동력원으로 그린 수소를 활용한 수소 연료전지가 대두되고 있다. 수소는 월등히 높은 중량 당 에너지를 가지며 연료전지를 활용할 시 높은 에너지 효율과 저피탐성을 보여 항공 분야로의 활용 가능성이 높은 것으로 기대받고 있으나, 부피 당 에너지가 낮고 저장이 용이하지 않는 등의 기술적 한계가 존재한다. 본 연구에서는 액체 수소 연료전지 항공기의 개념설계를 위한 성능 해석을 수행하여 임무 수행 능력을 분석한다. 국산 소형 항공기인 KC-100 을 기저 모델로 채택하여 프로펠러를 포함한 전기체 형상의 모델링을 수행하였다. 공력 및 추진 해석을 위하여 개념설계 단계에서 활용이 용이한 와류격자법을 채택하였다. 확보한 공력 모델을 검증하기 위하여 풍동 시험 결과를 해석적으로 재현하였으며, 그 결과를 상호 비교하였다. 이를 통하여 공력 모델의 해석 정확성을 검증하고 해석 결과를 보정하여, 항공기 성능 해석을 위한 공력 및 추진 데이터베이스를 구축하였다. 연료전지 추진 시스템의 중량 추정 모델을 확보하여 기저 모델 대비 전동화 기체의 중량 변화를 탐구하였고, 새로 도출한 중량을 바탕으로 전기 항공기의 성능 평가를 수행하였다. 연구에 활용한 임무 기준으로 약 45 kg 의 수소를 탑재하였을 때, 약 중량이 약 11% 증가함을 확인하였다.

주 요 어 : 액체 수소, 연료전지, 전동화, 전기 항공기, 개념설계
학 번 : 2021-22099